Unlocking Insights from Nerve Excitability Testing: Revealing Factors Shaping Nerve Health in Arm and Leg Data

by

Siyu Du

A thesis submitted in partial fulfillment of the requirements for the degree of

Master of Science

Faculty of Kinesiology, Sport, and Recreation

University of Alberta

Abstract

Introduction: The nerve excitability test (NET) assesses peripheral nerve properties, informing about nerve membrane integrity, ion channels, and axon function. Interpreting NET results is challenging due to the multitude of indices and their correlations. Exploratory factor analysis (EFA) offers a means to enhance interpretation by uncovering latent factors that link the measured indices.

Objective: We analyzed correlations among 30+ NET indices in upper and lower limb nerves of healthy adults, then used EFA to identify latent constructs. We also explored EFA's diagnostic potential for amyotrophic lateral sclerosis (ALS).

Methods: Healthy adults underwent NET on median and common fibular nerves. Correlations were assessed within and between nerves. EFA-identified factors were compared across groups and for relations to age and sex.

Results: 201 healthy participants and 15 people diagnosed with ALS were included. Correlations existed within, but not between nerves. EFA identified 4-5 factors per nerve. Factors reflected nerve excitability aspects affected by age and sex. One median nerve factor differed significantly between controls and people living with ALS.

Conclusions: Nerve excitability indices within a nerve are interdependent, but not between nerves. EFA effectively summarized indices and identified a potential ALS diagnostic factor.

Preface

This thesis is an original work by Siyu Du. The data used in this thesis were collected under multiple Research Ethics Board (REB) protocols: Population standards for nerve health (Pro00071524); Nerve excitability in people who use FES-assisted exercise (Pro00048262); Hudson Imaging Study (Pro00061945).

Acknowledgements

I want to express my heartfelt gratitude to my supervisor, Dr. Kelvin Jones, for not only mentoring me but also for infusing the entire process with enjoyment. His mentorship has played a crucial role in shaping both my academic and personal development. He not only possesses remarkable academic expertise but also a genuine passion for nurturing the potential of his students. His encouragement and guidance have been a constant source of inspiration, pushing me to strive for excellence in my work. His ability to provide constructive feedback and steer me in the right direction has been invaluable. I consider myself exceptionally fortunate to have had such an exceptional mentor.

I would like to extend my appreciation to Dr. Geri Ruissen for her willingness to join my supervisory committee. Her expertise in factor analysis and methodological insights were indispensable to the success of my research. Without her, the accomplishment of this research project would not have been possible. To Dr. Shintaro Kono, a member of my examining committee, I am grateful for his valuable feedback and constructive comments, which will undoubtedly guide my future work. His insights have been instrumental in refining my research. I am also appreciative of the valuable insights provided by Dr. Dave Collins and Dr. Yusuke Osaki regarding the neurophysiology aspect of my research. And I want to thank Dr. Michael Kennedy for being the chair during my examination. His thoughtfulness and support during the exam are truly appreciated.

I would like to express my sincere gratitude to the Faculty of Kinesiology, Sports and Recreation, which has provided me with a sense of belonging and support throughout my studies. It truly feels like home, thanks to the faculty's dedication to nurturing academic excellence. A special thank you to Elisha for her assistance and support from the very beginning.

Last but certainly not least, I would like to express my profound gratitude to my beloved family and many friends. Your unwavering support has been the bedrock of my academic journey, providing me with the strength and motivation to overcome challenges and reach for my goals. I couldn't have achieved what I have without you. Thank you for making this journey memorable and enjoyable.

Table of Contents

List of Tables

List of Figures

Chapter 1: Introduction

Excitability is essential to the ability of living tissue to respond to stimuli. In myelinated motor axons, excitability is determined by both active (i.e. ion channels) and passive (i.e. axon size and structure) characteristics in the nodal and internodal areas (Burke et al., 2001; Marmoy et al., 2019). The nerve excitability test (NET) utilizes the threshold tracking method to quantify nerve excitability and can provide insight into nerve health *in vivo* (Bostock et al., 1998). It has increasingly been employed in research and clinical settings to explore the electrophysiology of the axonal membrane and the underlying pathophysiology of neuromuscular conditions (Kiernan et al., 2020).

Several studies have investigated variations in excitability properties among nerves in both upper and lower limbs, revealing considerable heterogeneity within and between nerves (Bae et al., 2009; Klein et al., 2018; Kuwabara, 2001; Kuwabara et al., 2000, see Appendix, Table 1). However, the prevailing approach has been to treat the extensive set of over 30 indices derived from the NET as independent variables. While this methodology has provided insights, it tends to overlook the interconnected nature of many of these indices, which share common physiological mechanisms and exhibit concurrent alterations under different conditions. This suggests the presence of intercorrelations or underlying factors among these indices. By neglecting these interrelations and treating all indices as independent variables, there is a risk of introducing errors during analysis and interpretation, which could lead to the inadvertent identification of spurious results. This underscores the need for a more rigorous methodology to address these limitations.

Factor analysis is a widely used statistical technique employed to identify latent factors explaining interrelationships among observed/measured variables (Henson & Roberts, 2006). Within this statistical field, exploratory factor analysis (EFA) offers a data-driven approach to discovering latent factors, free from predetermined assumptions about their structure or loadings. Although factor

analysis has found extensive use in various fields, its application to neurophysiology remains relatively underexplored. In a single study focusing on nerve conduction, researchers identified five factors explaining 56% of the total variance across 28 variables, effectively distinguishing individuals with neuropathy (Robinson et al., 1992). This demonstrates the potential of factor analysis for clinical distinctions. Consequently, the application of EFA to NET data holds promise as an approach for interpreting nerve health more effectively.

One emerging application of NET is in the diagnosis and monitoring of lower motor neuron (LMN) diseases, such as amyotrophic lateral sclerosis (ALS). A meta-analysis identified seven NET indices as potential biomarkers of LMN degeneration in people diagnosed with ALS (Lugg et al., 2022). Understanding how factor scores derived from NET of the upper and lower limbs change may enhance the ability to detect changes associated with poor nerve health in those people.

In this study, we collected nerve excitability test (NET) data from a cohort of healthy adults, focusing on the motor axons of the median nerve at the wrist level and the motor axons of the common fibular nerve at the knee level. After addressing missing data, our analysis encompassed both intranerve and internerve correlation studies. Following this, EFA was applied to the datasets of the median and common fibular nerves, independently. The resultant factor scores, reflective of nerve excitability, were then compared between healthy control participants and individuals diagnosed with ALS. The objective was to ascertain whether this application of factor analysis to NET data can potentially augment our understanding of nerve excitability outcomes and their relevance to nerve health and disease-related variations.

Chapter 2 provides background information on NET and factor analysis. Chapter 3 describes the experimental and statistical methods employed in this research. The results of the project are discussed in Chapter 4, and Chapter 5 offers a comprehensive analysis of the findings, including their implications, limitations, and potential avenues for future research.

Chapter 2: Background

2.1 Physiological Basis of Nerve Excitability Tests

2.1.1 Nodal and internodal ion channels

In myelinated peripheral nerves, the axon is enveloped by Schwann cells, forming an

insulating myelin sheath (Glenn & Talbot, 2013). The axon consists of internodes, which are the

regions covered by myelin, and nodes of Ranvier, which are the periodic gaps between

internodes where the axon is exposed. Adjacent to the nodes of Ranvier are the paranodes, where

the myelin sheath is attached to the axon. The juxtaparanodes are located adjacent to the

paranodes, beneath the compact myelin (Figure 2.1). The distribution of ion channels within the

axon membrane varies between the nodes of Ranvier and the regions beneath the myelin sheath.
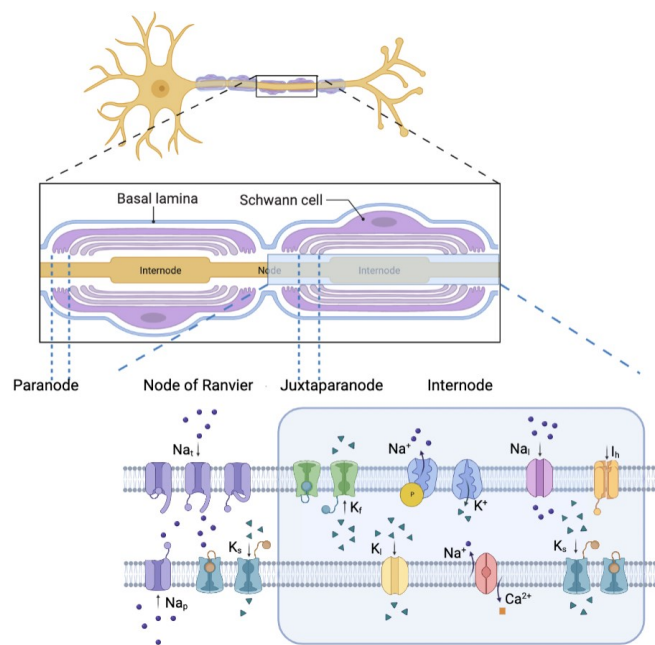
Figure 2.1 Structure of myelinated axon and the distribution of ion channels. Voltage-gated Na^+ channels, both transient (Na_t) and persistent (Na_p) channels are located at the node of Ranvier. K_s: Slow K^+ channels located at both the node and juxtaparanode. K_f: Fast K^+ channels. Na_l: Na^+ leak channel. K_l: K^+ leak channel. (Created with BioRender.com)

High density of voltage-gated sodium (Na^+) channels, specifically the $Na_v1.6$ subtype, are gathered at the nodes of Ranvier (Caldwell et al., 2000; Ritchie & Chiu, 1981). These Na^+ channels, which are sensitive to tetrodotoxin (TTX), play a crucial role in facilitating saltatory conduction along myelinated axons. Functionally, they can be classified into two types. Transient Na^+ channels (Na_t) rapidly open and inactivate, accounting for approximately 98% of the total Na^+ current (Burke et al., 2001; Crill, 1996). On the other hand, persistent Na^+ channels (Na_p) activate at more negative membrane potentials and exhibit slow inactivation, resulting in a sustained inward Na^+ current at the resting membrane potential (RMP) (Brown et al., 1994). It is believed that Na_p channels play a significant role in determining membrane polarization and, consequently, axonal excitability (Nodera & Kaji, 2006).

There are two main types of voltage-gated potassium channels expressed at the axon membrane according to their activation and deactivation kinetics: slow (K_s) and fast (K_f). K_s channels are found at the nodes of Ranvier and internodes (Baker et al., 1987; Devaux et al., 2004; Schwarz et al., 2006), while K_f channels are primarily located at the juxtaparanode (Chiu & Ritchie, 1984; Wang et al., 1993). While these potassium channels are open after depolarization, they are not directly responsible for repolarization, which is instead mainly determined by the inactivation and closure of sodium (Na^+) channels (Beckstein et al., 2003). K_f channels allow for fast repolarization of the membrane potential following an action potential, preventing the re-excitation of the node and ensuring the proper propagation of nerve signals. K_s channels contribute to the maintenance of the resting membrane potential (RMP) by facilitating the outward flow of potassium ions. Additionally, they play a significant role in reducing excitability after an action potential, thereby preventing repetitive firing and maintaining the overall stability of the nerve membrane (Kiernan & Lin, 2012). Mutations in these potassium

channel genes have been associated with peripheral nerve hyperexcitability (Spillane et al., 2016).

The Na^+/K^+ pump, also known as the sodium-potassium pump, actively transports three sodium (Na^+) ions out of the cell and two potassium (K^+) ions into the cell, utilizing ATP as an energy source (Skou, 1957, 1965). This process results in a net outward current of cations. While the precise localization of Na^+/K^+ pumps on the axonal membrane is not fully understood (Alberti et al., 2007), they play a critical role in restoring and maintaining the transmembrane gradients of Na^+ and K^+, as well as maintaining the RMP.

Another important ion channel is the hyperpolarization-activated cyclic nucleotide-gated (HCN) channel. These channels are primarily found at internodes and are unique in that they are activated by hyperpolarization. When the membrane becomes hyperpolarized, the HCN channels allow the influx of both sodium (Na^+) and potassium (K^+) ions, generating an inward current known as Ih. This current helps restore the hyperpolarized membrane to its RMP, thereby stabilizing the membrane potential and modulating excitability (Kubo et al., 2005). Among the four isoforms of HCN channels in humans, HCN1, HCN2, and possibly HCN3 are found in the peripheral nerve, while HCN4 is primarily located in the central nervous system (Doan et al., 2004; Marmoy et al., 2019). In cellular studies, the activation of HCN channels has been observed to occur with different time constants for each isoform: HCN1 activates with a time constant of 30 ms, HCN2 with 184 ms, HCN3 with 265 ms, and HCN4 with 461 ms (Moosmang et al., 2001).

Electrophysiological activities in nerves involve interactions among various ion channels. The excitability properties of nerves are not solely determined by a single type of ion channel. Instead, inferences about individual channel activity are based upon the complete set of

excitability measurements obtained through NET. By stimulating the nerve with various combinations of conditioning and test pulses, a NET provides valuable insights into the complex interplay of ion channels and their contributions to nerve function.

The standard protocol for nerve excitability test, known as the TROND protocol, was initially developed in Trondheim, Norway in 1999 (Kiernan et al., 2000). This protocol encompasses five subtests that are recorded in a specific sequence: stimulus-response, strength-duration, threshold electrotonus, current-threshold relationship, and recovery cycle (Figure 2.2).

2.1.2 Stimulus-response curve

NET employs the threshold tracking technique, whereby the stimulus strength needed to evoke a predetermined compound muscle action potential (CMAP) size, referred to as the threshold, is measured and recorded throughout the procedure (Bostock et al., 1998; Kiernan et al., 2020). The relationship between the stimulus intensity applied to the nerve and the resulting muscle response (CMAP) is essential for evaluating the threshold in nerve excitability.

To establish the stimulus-response curve, the maximal CMAP ($CMAP_{max}$) is first obtained by progressively increasing the stimulus current manually. Subsequently, the program automatically records the responses using 1ms long test stimuli with 6% stepwise decrements. The resulting stimulus-response (SR) plot (Figure 2.2A) demonstrates that as the stimulus intensity increases, the amplitude of the CMAP also increases until it reaches its maximum, indicating the muscle recruitment ceiling. The SR plot can be normalized into a relative SR plot (Figure 2.2B) to accommodate individual differences. This involves expressing the response as a percentage of $CMAP_{max}$ and plotting the stimulus current relative to the current needed to generate 50% of $CMAP_{max}$. This process improves the accuracy and optimizes the threshold
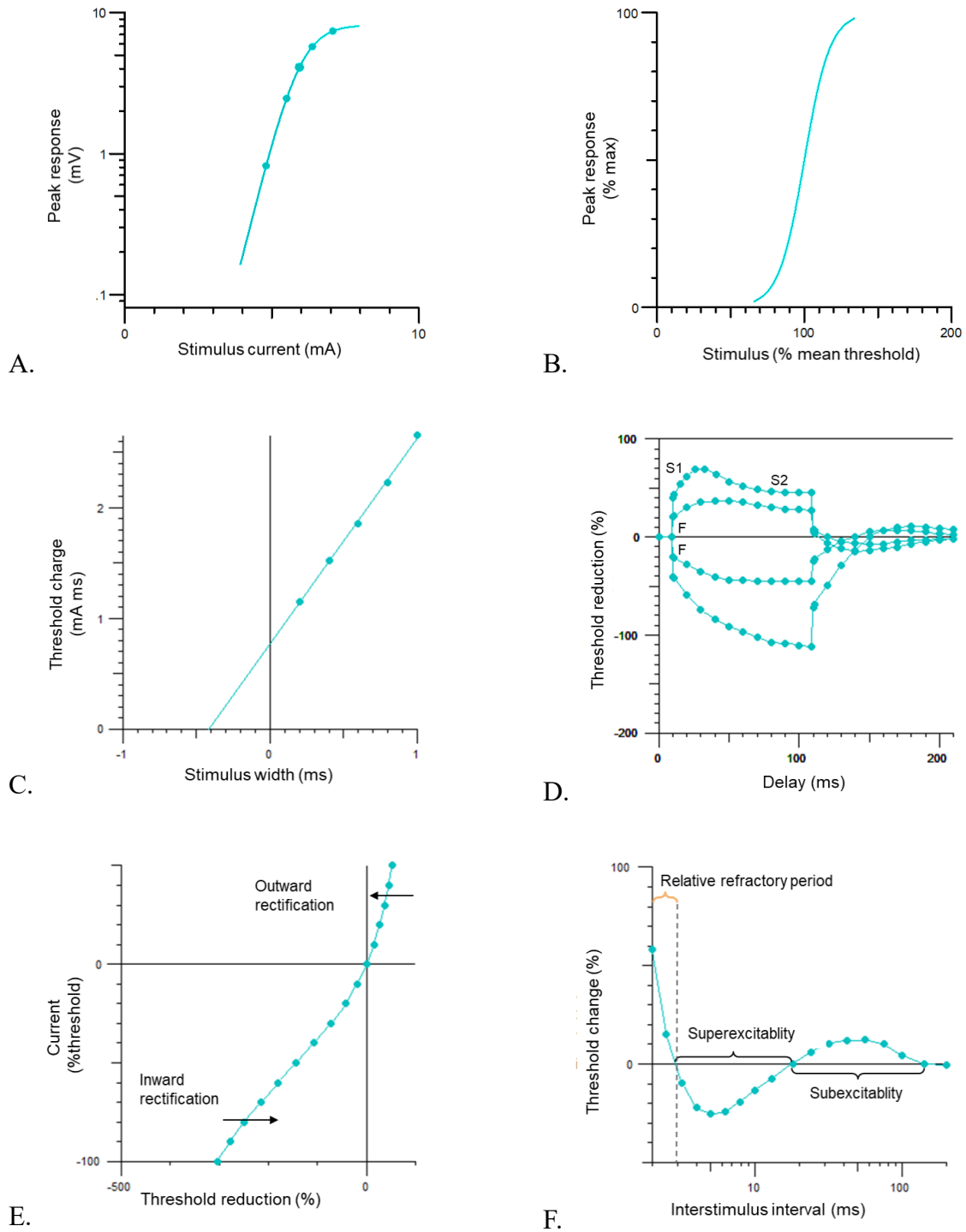
Figure 2.2 Five subtests in the TROND protocol of nerve excitability test. A. stimulus-response curve. B. relative stimulus-response curve. C. strength-duration curve. D. threshold electrotonus. E. current-threshold relationship. F. recovery cycle. (Figures adapted based on QTracP plots)

tracking method in the subsequent excitability subtests.

The main objective of the stimulus-response subtest is to determine the submaximal target response and the slope of the stimulus-response curve for optimizing the threshold tracking (Kiernan & Lin, 2012). The target size for the CMAP is commonly set at 30-40% of $CMAP_{max}$, which corresponds to the steepest portion of the stimulus-response curve and exhibits the highest responsiveness to changes on both sides (Kiernan et al., 2020). The ends of the curve are less responsive to changes, requiring larger current adjustments for minor potential changes. In certain excitability subtests (threshold electrotonus and current-threshold relationship), where a long-duration conditioning current is applied, it is crucial for axons to remain subthreshold and prevent action potential generation during this time to ensure accurate measurements. To achieve this, a lower target CMAP is used. Axons with a flatter stimulus-response slope, such as sensory axons compared to motor axons, are more likely to respond during the conditioning current (Burke et al., 2007).

2.1.3 Strength-duration relationship

The relationship between strength and duration can be described by the equation:

$$Q = I \cdot t$$

Where Q is the stimulus charge; I is the stimulus current; t is the duration of the pulse. In this equation, the threshold current for a stimulus of infinite duration is called rheobase, which is a reflection of nodal membrane excitability. Weiss (1901) indicated that the stimulus charge is proportional to the rheobase, which is known as Weiss's empirical law:

$$Q = I_{rh} (t + \tau_{SD})$$

where τ_{SD} is the strength duration time constant (SDTC), also known as chronaxie, and has a value in the range of 450-600μs in normative human axons (Burke et al., 2001; Kiernan et al.,

2020). SDTC partly depends on the nodal persistent Na^+ conductance active at the resting membrane potential (Bostock & Rothwell, 1997).

By examining the linear relationship between stimulus charge and stimulus duration, both rheobase and SDTC can be determined from a stimulus charge-duration plot (Figure 2.2C) using five different stimulus widths (0.2, 0.4, 0.6, 0.8, and 1 ms). SDTC is obtained from the x-intercept of the fitted straight line, while the slope of this relationship corresponds to the rheobase (Kiernan & Lin, 2012).

2.1.4 Threshold electrotonus and Current-threshold relationship

The long-duration (100-200 ms) conditioning currents can alter the potential in the internode membrane and subsequently alter the nerve excitability (Nodera & Kaji, 2006). Threshold electrotonus assesses the changes in membrane potential during a subthreshold current (usually 20% and 40% of the current used to generate the target response, e.g. 40% of $CMAP_{max}$) using test pulses large enough to get the predetermined target response. It provides information on the axon's accommodation to depolarization and hyperpolarization.

The proportional change in threshold immediately after a conditioning current is applied (F phase) results from the cable properties of the membrane. This phase exhibits a relatively symmetric response to conditioning pulses of the same magnitude (e.g., +40% and -40%) during depolarization and hyperpolarization. A decrease in threshold is represented by an upward deflection in the graph, while an increase in threshold is indicated by a downward deflection (Figure 2.2D). Following the initial F phase, a depolarizing current leads to a slight decrease in the threshold (upward S2 phase) due to the activation of K_f channels of the K_v1 (KCNA) family. The subsequent decline in depolarizing electrotonus is attributed to the opening of K_s channels of the K_v7 (KCNQ) family (Baker et al., 1987; Kiernan et al., 2020). After the conditioning current

stops, there is a slow undershoot period with an increased threshold due to the slow deactivation of K_s channels.

In a hyperpolarizing threshold electrotonus, the threshold continues to increase or excitability decreases (downward S2 phase) after the initial drop in the F phase, resulting from the deactivation of partially open K_s channels at rest. Subsequently, HCN channels (depending on the isoforms present, HCN 1-4) gradually open, allowing the hyperpolarization-activated current Ih to flow and increase excitability. When the conditioning current concludes at 100ms, there is a gradual decrease in threshold followed by an overshoot above the baseline due to the slow deactivation of HCN channels and the recovery of persistent Na^+ channels. (Kiernan et al., 2020).

To further explore the accommodative properties in axons, threshold changes resulting from changing conditioning current (from -100% hyperpolarization to 50% depolarization) can be plotted as an analogue of the current-voltage (I/V) relationship (Figure 2.2E), called the current-threshold relationship (Threshold I/V) (Kiernan et al., 2020). Instead of giving a test stimulus during the 100 ms conditioning current, the protocol of current-threshold relationship utilizes varying strength of conditioning current with a fixed duration of 200ms. The slope of the curve in the hyperpolarizing direction reflects the degree of inward rectification due to I_h current activation. While in the depolarizing direction, the slope reflects the outward rectification due to the K^+ currents (Nodera & Kaji, 2006). The resting I/V slope, which is the slope of the threshold I/V curve around zero conditioning current, reflects the resting input conductance and is dependent on the channels open at resting membrane potential (Kiernan et al., 2020).

2.1.5 Recovery cycle

Following the passage of an impulse, a sequence of excitability changes occur in the axonal membrane, known as the recovery cycle. This cycle consists of four periods in chronological order: the absolute refractory period (ARP), relative refractory period (RRP), superexcitability period, and subexcitability period. To assess the recovery process, suprathreshold conditioning pulses and test pulses are paired at varying intervals (Bostock et al., 1998). The changes in the threshold required to elicit a target response are recorded over time (Figure 2.2F).

The refractory period immediately after the depolarization of the conditioning pulse lasts 3-4ms. It has been demonstrated that the inactivation and slow recovery of Na^+ channels are responsible for most of the refractoriness in normal myelinated axons (Schwarz et al., 1995). A greater stimulus is required to elicit a response.

Immediately following the refractory period is the superexcitability phase, during which the axon excitability increases and the threshold decreases. Current pathways in the cytoplasm of Schwan cells around the internodes, or Schmidt Lanterman incisures, allow the charge on the internodes' capacitance to flow to the nodes generating a depolarizing afterpotential (Barrett & Barrett, 1982) resulting in the superexcitable phase. Superexcitability depends on the polarization state of the membrane. Hyperpolarization induces more closure of fast K^+ channels, giving rise to an increase of the depolarizing afterpotential and thereby the superexcitability. Conversely, depolarization opens K^+ channels and reduces superexcitability. This period usually peaks around 5-7ms and ends 15-20 ms after the initial conditioning pulse.

At last, the late subexcitability period is indicative of hyperpolarization in the axons and disappears once resting membrane potential is re-established. It reflects the balance between the

gradual decaying of slow K^+ current as well as superexcitability (Kiernan et al., 2020). The peak

of subexcitability was approximately 35ms and then slowly returned to resting state at around

200ms. This process does not directly reflect the activities of K_s channels but may imply

extracellular K^+ levels (Kiernan & Lin, 2012).

In summary, the measures obtained from the NET offer a comprehensive understanding

of the membrane properties at the stimulation site. They provide valuable insights into the

physiological processes underlying nerve excitability and conduction, making them relevant for

studying excitability disorders and demyelinating conditions (Nodera et al., 2006).

2.2 Influencing Factors of Nerve Excitability in Healthy Population

NET assesses membrane properties by analyzing over thirty quantitative indices, which

can be influenced by both biological and technical factors to some extent.

2.2.1 Demographic characteristics

Several prior studies have investigated NET results in healthy human controls, aiming to

provide reference data for the test and explore the effects of demographic features (age, sex and

body mass index) on the ionic properties of peripheral motor axons (Bae et al., 2008; Casanova

et al., 2014; Jankelowitz et al., 2007; McHugh et al., 2011; see Table1).

With increasing age, several effects have been reported in multiple studies, including a

decrease in superexcitability, a decline in the stimulus-response slope, and a reduction in the

threshold change following strong hyperpolarizing currents. These age-related changes have

been attributed to variations in the expression of specific channels, particularly voltage-gated K_s

channels (KCNQ), and potential age-related alterations within the nerve (McHugh et al., 2011).

They suggest a decline in nerve health as individuals get older. A recent meta-analysis from our

lab, of five studies with a total of 340 participants ranging in age from 18 to over 80 years of age,

suggests that superexcitability is the only NET outcome measure that significantly changes with age (unpublished observation).

Sex has equivocal effects on nerve excitability; the findings across studies are variable. Some studies report females to have a lower threshold (rheobase) than males and a slight increase in superexcitability (Bae et al., 2008; McHugh et al., 2011). There are also differences in certain KCNQ-mediated properties, such as late subexcitability, accommodation half-time, and threshold undershoot following depolarizing electrotonus, suggesting a greater expression of nodal KCNQ channels in females. But many of the studies are small and inconclusive.

BMI was not found to have a significant influence on nerve excitability data or explain sex-related differences in the threshold (McHugh et al., 2011). It is not a prominent factor in nerve excitability measurements and does not contribute significantly to the observed variations in the threshold.

2.2.2 Anatomical factors

Electrical stimulation is influenced by axon diameters (Baker et al., 2000). The variance in fiber diameter may increase the range of thresholds, altering the excitability of nerves such as the stimulus intensity, and rheobase. Axon size has been reported to affect the refractory period of single human afferents (Brink & Mackel, 1993). But it alone would not cause the RRP difference between nerves (Kuwabara et al., 2000).

The site of stimulation along the nerve could also affect excitability results. The variations are likely attributed to differences in the internodes at different locations along the nerve (Kuwabara et al., 2000). Furthermore, variations in membrane and nodal ion conductances may contribute to differences in excitability between different muscles innervated by the same nerve (Bae et al., 2009; Jankelowitz & Burke, 2009).

2.2.3 Serum potassium level

Membrane excitability properties are influenced by the electrolyte environment, especially K^+ concentration. In healthy humans, relative refractory period, superexcitability, and threshold electrotonus are strongly correlated with serum K^+ levels (within normal physiological range) (Boerio et al., 2014; Kuwabara et al., 2007). Specifically, the relative refractory period increased, superexcitability decreased and a relative "fanning-in" pattern of threshold electrotonus at higher K^+ levels, which are consistent with the relative increase in depolarization of axonal membrane by higher extracellular K^+ concentration (Boerio et al., 2014; Kuwabara et al., 2007). These changes were also found in hyperkalemia which resembles membrane depolarization (Kiernan et al., 2002; Z'Graggen & Bostock, 2008).

2.2.4 Temperature

Temperature can alter the kinetics of ion channels due to thermodynamic properties and subsequently change the axonal membrane potential. In experimental settings, hypothermia causes excitability changes that resemble membrane depolarization while hyperthermia induces hyperpolarizing axon stress (Kovalchuk et al., 2018; Marmoy et al., 2019). Specifically, the relative refractory period was significantly prolonged with superexcitability disappearing at 20℃ (Kiernan et al., 2001; Kovalchuk et al., 2018). The accommodation half-time, resting and minimum I/V slope increased with cooling temperature in the median nerve (Kiernan et al., 2001; Kovalchuk et al., 2018). The influence of temperature on the nerves of the upper and lower limbs is similar (Marmoy et al., 2019).

Due to the sensitivity of nerve excitability to temperature, especially in the recovery cycle, the same range of temperature should be maintained to obtain meaningful comparisons within or between subjects or groups (Kiernan et al., 2001).

2.2.5 Experimental factors

Proper skin preparation to reduce impedance as well as optimized placement of stimulating and recording electrodes are important in the matter of the lowest threshold, or rheobase (Kiernan et al., 2020). Prolonged high-frequency stimulation of the peripheral nerve would not only cause paraesthesia in participants but also lead to activity-dependent changes in nerve excitability, such as a prolonged superexcitability period in motor axons (Bostock & Bergmans, 1994; Kiernan et al., 1997; Luu et al., 2021). Therefore, stimulus frequency should be adjusted to below 3Hz to avoid the cumulative effect. Ischemia will induce a depolarizing effect on the axon excitability and thus the condition of the limbs should be monitored during the experiment to prevent unexpected pressure (Lin et al., 2002; Mogyoros, 1997).

Nerve excitability properties are influenced by various factors that collectively contribute to their overall effects. There may be some correlation between indices that change with the same factor.

2.3 Differences in Excitability Indices between Nerves in Upper and Lower Limbs

Differences in nerve excitability indices between upper and lower limb motor axons can be attributed to the distinct functional demands placed on the muscles in these regions. For example, hand muscles are more involved in fine motor functions and leg muscles play important roles in gross motor functions. As a result, excitability testing showed distinct patterns in the upper and lower limbs (Klein et al., 2018) (see Appendix, Table 1).

Comparisons between median and common fibular motor axons have revealed distinct characteristics. Median motor axons exhibit notable features such as greater S2 accommodation, a more pronounced undershoot to depolarization, and increased late subexcitability. These findings suggest the presence of a higher nodal and internodal slow K^+ conductance (Klein et al.,

2018; Kuwabara, 2001; Kuwabara et al., 2000). In contrast, lower limb axons demonstrate less superexcitability (Klein et al., 2018), indicating a higher fast K^+ conductance or decreased internodal capacitance. This discrepancy may contribute to reduced depolarization afterpotential, subsequently leading to decreased slow potassium activation and subexcitability. (Baker et al., 1987; Barrett & Barrett, 1982).

Lower limb axons also exhibit a smaller increase in threshold 90–100 ms after hyperpolarizing current compared to upper limb axons (Klein et al., 2018). This difference becomes more pronounced during the S3 phase of hyperpolarization when the limbs are subjected to warming, acting as a hyperpolarizing stress (Marmoy et al., 2019). It was suggested that slower isoforms of hyperpolarization-activated cyclic nucleotide-gated (HCN) channels, likely HCN2 and HCN3, are more expressed in lower limb axons. This results in a greater inward rectifying current (Ih) during constant hyperpolarization, leading to greater accommodation compared to the upper limb (Marmoy et al., 2019). Such variations in the lower limb axons allow for higher firing rates, which are crucial for postural control and weight-bearing activities.

2.4 Utility of Nerve Excitability Indices as Biomarkers for People Diagnosed with ALS

Amyotrophic lateral sclerosis (ALS) is a neurodegenerative disorder affecting both upper motor neurons (UMNs) and lower motor neurons (LMNs) (Rowland & Shneider, 2001). It is characterized by the progressive degeneration of these neurons in the brain and spinal cord. Timely diagnosis and effective monitoring of disease progression are vital for understanding ALS pathophysiology and evaluating potential therapies. The NET has emerged as a promising non-invasive tool for evaluating nerve health, with certain indices showing potential as biomarkers for individuals diagnosed with ALS.

The strength of NET in the ALS context lies in its ability to detect subtle changes in nerve excitability before the onset of clinical symptoms (Bostock et al., 1995). Several studies have demonstrated altered nerve excitability indices in ALS cohorts in comparison to their healthy counterparts. A comprehensive meta-analysis conducted by Lugg et al. (2022) revealed a select group of seven specific excitability indices: TEd(90–100ms), strength-duration time constant (SDTC), superexcitability, TEd(40–60ms), resting I/V slope, 50% depolarizing, and subexcitability, that exhibit the potential to differentiate people diagnosis with ALS from the healthy population. Notably, four NET indices – TEd(10–20ms), TEd 90–100 ms, superexcitability, and SDTC – demonstrated promise as early biomarkers for ALS. However, the comprehensive nature of the meta-analysis is limited by data availability from primary studies. Specifically, only 16 out of over 30 NET indices were reported in four or more studies. This leaves a significant proportion of NET indices unexamined. Furthermore, the mean and standard deviation values extracted from primary studies lack individual-level correlations between NET indices. This approach treats each index as an independent variable, ignoring interdependencies originating in shared anatomical and physiological factors. The absence of standardized reporting and inter-index correlations introduces some uncertainty about the diagnostic potential of unexamined indices. This gap suggests an opportunity for advancement: an approach that accounts for the latent factors connecting the 30+ NET indices. By capturing these relationships, this approach could enhance the diagnostic utility of NET in ALS.

NET also shows promise in monitoring disease progression and assessing the efficacy of therapeutic interventions in ALS. Longitudinal studies using NET have demonstrated increasing threshold electrotonus changes over time, reflecting the ongoing neurodegeneration in ALS

(Cheah et al., 2012). These changes may serve as objective markers of disease progression and offer insights into disease-modifying treatments.

Furthermore, NET has the potential to provide insights into the mechanisms underlying ALS in vivo. By examining the correlation patterns between various nerve excitability parameters, researchers have gained insights into the involvement of specific ion channels and membrane properties in ALS pathophysiology. For example, studies suggest that prolonged SDTC, increased superexcitability and abnormalities in threshold electrotonus may be caused by increased sodium (Na^+) channel conductance, and decreased fast and slow potassium (K^+) in ALS (Bostock et al., 1995; Geevasinga et al., 2015; Kanai et al., 2006). However, a broader reduction in ion channels, possibly due to disruptions in protein homeostasis, is also proposed to contribute to these abnormalities (Howells et al., 2018).

In conclusion, NET holds promise as a valuable ALS biomarker. Its non-invasive nature, early change detection capability, and potential for monitoring disease progression make it a valuable tool in ALS research and clinical practice. By providing insights into nerve membrane properties and ion channel activities, NET contributes to our understanding of ALS pathophysiology and may facilitate the development of targeted therapeutic interventions.

2.5 Exploratory Factor Analysis (EFA): Unveiling Latent Factors in Nerve Excitability Indices

A methodological gap was identified in the preceding discussion when considering the analysis of the multiple nerve excitability test (NET) indices in the context of ALS. We posited that a more robust methodology, one that takes into account the underlying latent factors interconnecting the 30+ NET indices, could enhance the interpretation of test results. This approach would implicitly address the shared anatomical and physiological factors that underlie various indices, providing a more comprehensive understanding of nerve health and function. Factor analysis emerges as a suitable approach to achieve this goal. It can be used to determine

the unobservable dimensions or constructs that account for the correlation pattern among measures (Fabrigar & Wegener, 2011).

2.5.1 Introduction of the common factor model

The origin of the factor analysis model can be traced back to the early 20th century when (Spearman, 1904) proposed a two-factor theory to interpret psychological tests, differentiating between a "general" factor representing overall intelligence and "specific" factors unique to each variable. However, this initial work differs from the later developments in the field, as modern factor analysis typically involves multiple factors. The majority of modern factor analysis methodologies derive from Thurstone's (1934, 1947) *Multiple Factor Analysis Model*, now commonly referred to as the *common factor model*.

The common factor model is the foundation of factor analysis. In contrast to the principal component model used in the principal component analysis (PCA), which intends to reduce the original variables into a new set of uncorrelated principal components while retaining the maximum variance possible, the common factor model represents the underlying structure of correlations by assuming that the observed/measured variables are influenced by a smaller number of unobserved (latent) factors. These factors are not directly measured but are inferred from the observed variables based on their patterns of covariance. Exploratory factor analysis (EFA) aims to discover the number and nature of these latent factors (DeCoster, 1998).

Within this framework, the model proposes the existence of both common factors and unique factors to explain the relationships between these measured variables (Figure 2.3). Common factors are unobservable constructs that exert linear influences on multiple measured variables. These factors account for the shared variance among variables and represent the underlying latent constructs. Unique factors, in contrast, are also unobservable sources of

influence, but only affect that is specific to individual variables and not shared among other variables.
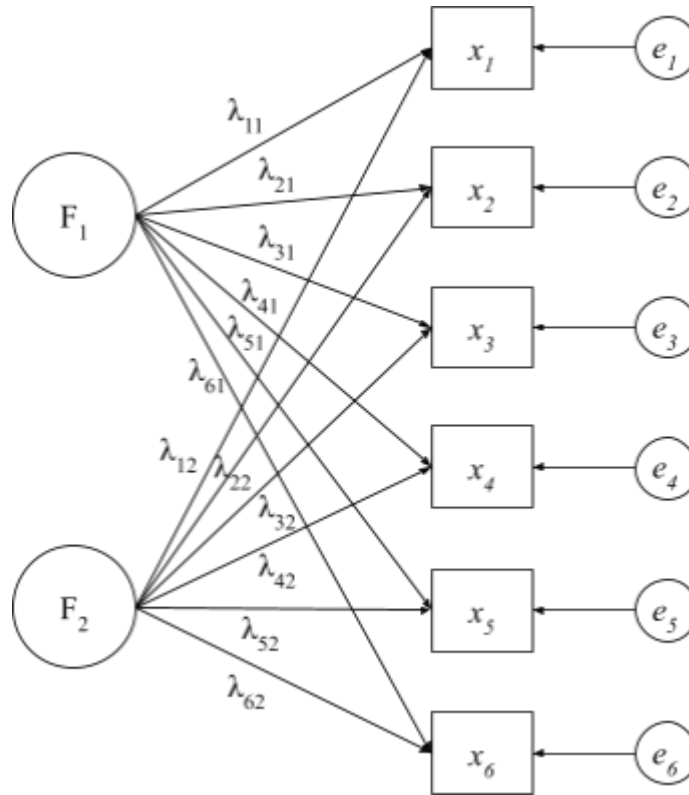
Figure 2.3 Common Factor Model (adapted from DeCoster, 1998). Each observed/measured variable (x_1 through x_6) is influenced by a combination of underlying common factors (F_1 and F_2) and underlying unique factors (e_1 through e_6). λ_{ij} represents the factor loading (strength of link) of the jth factor to the ith variable. The factor loading between each factor and each measure varies, with certain measures being more influenced by a particular factor than others.

Importantly, the common factor model allows for a meaningful partitioning of the variance within measured variables. The observed variance can be conceptually divided into two components: common variance and unique variance. Unique variance can be further partitioned into specific variance and error variance. Specific variance is repeatable and arises from the characteristics of individual variables, whereas error variance is random and may impact the reliability of the measured variable (Kline, 2013). Researchers often refer to the common variance by its proportion relative to the total variance in the measure that is explained by the

common factors, termed communality (Child, 2006). For each variable, communality is calculated as the sum of its squared factor loadings.

The simplest factor model can be represented mathematically as follows:

$$X = \Lambda f + e \quad (1)$$

where X is the matrix of n x p observed variables (n = number of cases, p = number of observed variables). Λ is the p x k matrix of factor loadings (k = number of factors), indicating the relationships between the observed variables and the underlying factors. Higher factor loadings suggest a stronger association. f is the n x k matrix of common factors. e is the vector of unique or error terms, capturing the unexplained variance in the observed variables.

After identifying the factor model, the factor scores can be calculated from the factor loadings. Factor scores in factor analysis are numerical values that represent the estimated scores of each individual or observation on the underlying factors. The regression method gives maximal validity when factor scores are correlated to the estimated factors (DiStefano et al., 2009). An equation can be represented as

$$F = ZB \quad (2)$$

where F is the n x k matrix of factors scores, representing the values of the latent factors for each observation. Z is the n x p matrix of standardized observed variable scores. B is the p x k matrix of factor score coefficients. Factor score coefficients for estimating factor scores from variable scores are a product of the inverse of the correlation matrix and the factor loading matrix.

Factor scores can be used in further analyses to examine group differences or to include factor information in regression models.

2.5.2 Ratinale and benefits of using factor analysis in nerve excitability testing

While the origins of factor analysis lie within psychology, its utility extends into diverse domains including social sciences and biostatistics. This method demonstrates its potential to effectively model datasets where continuous variables exhibit linear relationships with a limited set of latent factors (Jolliffe, 2005). However, its applicability in neurophysiology testing, particularly within the realm of nerve excitability assessment, has not been fully investigated.

The field of nerve excitability testing aims to unravel the intricacies of nerve functioning through the evaluation of electrophysiological responses. This involves the measurement of multiple nerve excitability indices, which provide insights into ion channel activity, nerve membrane characteristics, and other physiological properties. Traditionally, researchers have treated these indices as independent variables, potentially overlooking the interdependencies and shared underlying factors that bind them. This oversight may lead to redundancy, complicating the analysis and interpretation of large datasets.

EFA provides a statistical tool for identifying the latent constructs, moving beyond expert intuition. Notably, a study by Robinson et al. (1992) explored EFA for nerve conduction studies, successfully revealing physiologically meaningful factors from a comprehensive array of 28 indices. This achievement highlights EFA's potential in extracting essential factors, thus enhancing our ability to make sense of complex neurophysiological datasets. Factors, such as conduction velocities, sensory amplitudes, and ulnar/median/peroneal functions, emerged, aiding in the distinction between diabetic and control groups. Such applications demonstrate EFA's potential for polyneuropathy investigations and offer a pathway to streamline the analysis of extensive clinical data.

The complexity of the nerve excitability test (NET) outcomes can be overwhelming due to the multitude of indices. With over 30 indices, the risk of redundancy and confusion in individual analysis is evident and poses challenges for routine clinical application. The identification of shared physiological factors among these indices, suggests the presence of underlying correlations or common factors. EFA provides a tool to detect coherent patterns embedded within groups of indices (e.g. ion conduction, membrane properties) that are not directly measured. Each factor influences multiple nerve excitability indices simultaneously. These factors possess the potential to decipher the complexity of NET indices, simplifying comprehension and enhancing the clinical relevance of nerve excitability tests.

Historically, the interpretation of the array of indices generated by a NET has been based on insights from *in-vitro* studies or theoretical models (Jensen et al., 2008; Kiernan et al., 2020). It's noteworthy that modifying a single condition, like altering the conduction of a specific ion channel, results in changes across multiple NET indices, hinting at the presence of a shared factor influencing these indices. Moving forward, if future research can establish a direct link between changes in ion channel conduction or nerve membrane properties and the observed shifts in EFA-derived factors, it would improve our understanding of the mechanisms underlying nerve excitability. This connection would further solidify the relevance and validity of the factors identified through EFA, providing valuable insights into the physiological processes influencing nerve health and function.

In summary, EFA emerges as a promising tool for identifying the underlying constructs with nerve excitability testing and the resulting indices. While a single study offers preliminary insights into EFA's relevance, further research in this area is warranted to fully explore the utility of EFA in NET and its potential impact on clinical practice and patient outcomes.

2.5.3 Considerations before undertaking an exploratory factor analysis

Before embarking on an EFA with NET data, it is necessary to ensure that the data are suitable for this technique. The quality of EFA results is linked to the quality of the input data, making this preliminary assessment crucial. A series of critical considerations should be taken into account, aligning both with the characteristics of the measured variables and the sample (Fabrigar & Wegener, 2011).

Factor analysis is typically applied to continuous or ordinal variables (Tabachnick & Fidell, 2007). Addressing missing values requires careful consideration of their impact on sample size, particularly when they are missing not at random, with removal of cases usually necessary to prevent potential overestimation (Tabachnick & Fidell, 2007). It's essential to ensure a correlation coefficient (r) of at least .30 to indicate a reasonable relationship between variables (Tabachnick & Fidell, 2007). Also, assess the dataset for extreme collinearity, also known as multicollinearity, characterized by a high correlation between indices (Dormann et al., 2013). Multicollinearity can result in unstable factor loadings, challenges in factor interpretation, increased standard errors, and reduced model fit, thereby undermining the reliability and interpretability of the results (Kyriazos & Poga, 2023).

To conduct a robust factor analysis, several assumptions must be satisfied. These include the assumptions of univariate and multivariate normality within the dataset, as well as the absence of univariate and multivariate outliers (Field, 2009). Also, the model is based on the assumption of a linear relationship between common factors and variables during correlation computation (Fabrigar & Wegener, 2011). For something to be considered a factor, a minimum of three variables is typically required to extract reliable factor structures, though this criterion is subject to study design (MacCallum et al., 1999; Tabachnick & Fidell, 2007). Interpretation of

rotated factors with merely two variables should be approached cautiously. Such cases are deemed reliable only if these variables demonstrate a strong intercorrelation ($r > .70$) while exhibiting minimal correlation with other variables (Yong & Pearce, 2013).

EFA is generally considered a "large-sample" method. There are various guidelines for determining an appropriate sample size, including using a ratio of 5 or 10 cases per variable and a total minimum sample size of 100–200 observations (Gorsuch, 1983; Everitt, 1975; Nunnally, 1978; Comrey & Lee, 1992). However, subsequent research suggested significant flaws in these guidelines, as they lack sensitivity to a variety of data characteristics (Fabrigar et al., 1999; MacCallum et al., 1999, 2001). The adequacy of the sample size depends on the quality of the data, with stronger data allowing for smaller sample sizes (Fabrigar et al., 1999; MacCallum et al., 1999). Strong data in factor analysis demonstrates a clear and reliable structure, characterized by high communalities, minimal cross-loadings (a variable that loads at .32 or higher on two or more factors), and having multiple variables strongly load on each factor (MacCallum et al., 1999). An example of conceptualizing the process for determining sample size can be found in Table 2.1. But a larger sample size is always preferred. Additionally, a heterogeneous sample is recommended over a homogeneous one, as the latter have lower variance and factor loadings (Kline, 1994).

Table 2.1 Sample size determination for model fitting procedure in exploratory factor analysis (Fabrigar & Wegener, 2011).

Condition	Communalities	Variables per factor	Sample size
Optimal	≥0.7	3–5	100
Moderate	0.4–0.7	≥3	200
Poor	<0.4	≥2	≥400

Note: Under poor conditions, an even larger sample size might still prove insufficient.

In the context of NET data, these considerations lay the foundation for a rigorous and insightful EFA, ensuring that the subsequent interpretation and insights extracted from the analysis reflect the underlying factors of nerve excitability indices.

Given the complex interplay of the NET indices, the observed disparities between arm and leg NET data, and the potential benefits of EFA in identifying latent constructs, this study is primarily aimed at examining the correlations among NET indices and assessing the applicability of EFA in analyzing NET data obtained through the TROND protocol. Additionally, this study aims to address secondary questions regarding the influence of age and sex on the factor scores and explore the diagnostic utility of EFA-derived factors in differentiating between people with ALS and healthy controls.

Chapter 3: Methods

3.1 Experiment Methods and Procedures

3.1.1 Healthy control group

Healthy adults aged 18 or older were recruited. The Michigan neuropathy screening instrument was used to screen for peripheral neuropathy (Feldman et al., 1994). Additional exclusion criteria included: 1) entrapment neuropathies such as carpal tunnel syndrome; 2) prior trauma or surgeries that could cause peripheral nerve injuries; 3) prior chemotherapy treatment; 4) other chronic diseases (i.e. diabetes) or medications (i.e. some kinds of antibiotics, cardiovascular or central nervous system acting drugs) that are associated with peripheral nerve disorders.

This is a cross-sectional study that combines all the available data collected in the Clinical and Theoretical Neurophysiology (CTN) Lab. The data were collected under multiple Research Ethics Board (REB) protocols: Population standards for nerve health (Pro00071524); Nerve excitability in people who use FES-assisted exercise (Pro00048262); Hudson Imaging Study (Pro00061945). Prior to their participation, all individuals provided written informed consent. Demographic and clinical information, such as sex, age, medical history, and other relevant details, were recorded for each participant.

The number of participants needed to detect a correlation of medium effect size (i.e. $r = 0.3$, with an alpha of 0.05 and power of 0.8) is 85 (Browner et al., 2022). There were 201 healthy controls included, which is appropriate for correlation analysis, with the capacity for generalizability. Regarding the suitable sample size for EFA, 160 is recommended for a 5: 1 participant-to-variable ratio or 320 for a 10: 1 ratio, given the 32 NET indices (Everitt, 1975;

Gorsuch, 1983; Nunnally, 1978). In this study, we utilized the 201 cases and assessed the adequacy throughout the analysis.

We usually chose the right side to study unless the participant had a recent or former injury in the right limbs or skin wounds at the stimulating sites.

3.1.2 ALS group

The data collected from people with ALS in the CTN Lab was initially intended for a neurophysiology biomarker study. We selected a subset of this data to analyze and compare certain variables or parameters. The inclusion criteria were: 1) diagnosis of ALS according to the Revised El Escorial criteria, see Table 3.1 (Brooks, 1994); 2) Forced vital capacity (FVC) > 60%.

Table 3.1 Revised El Escorial classification of ALS

Diagnostic category	Inclusion criteria
Definite ALS	Presence of upper motor neuron and lower motor neuron signs in three anatomical regions
Probable ALS	Presence of upper motor neuron and lower motor neuron signs in at least two regions with upper motor neuron sign rostral to lower motor neuron signs
Probable ALS, laboratory results supported	Presence of upper motor neuron and lower motor neuron signs in one region with evidence by EMG of lower motor neuron involvement in another region
Possible ALS	Presence of upper motor neuron and lower motor neuron signs in one region or upper motor neuron signs in two or three regions, such as monomelic ALS, progressive bulbar palsy, and primary lateral sclerosis

Note: Four anatomical regions are: bulbar, cervical, thoracic, and lumbar.

Exclusion criteria: invasive ventilation or any other conditions that were specified as exclusion criteria for the healthy control group.

People who meet the criteria were invited to participate. All participants need to provide written informed consent before being involved in the study (Research Ethics Board, University of Alberta, Hudson Imaging Study - Pro00061945). Demographic and clinical characteristics (sex, age, time of onset, ALS region of onset, time of diagnosis, family history, relevant medication, etc.) of the patients were recorded. The functional status of the patients was measured using the revised ALS Functional Rating Scale (ALSFRS-R) (Cedarbaum et al., 1999).

The selection of the side for each patient was determined based on clinical judgment. The general principle was to choose the side opposite to the side of onset, or the strongest side as evaluated using the Medical Research Council (MRC) scale for muscle strength (Medical Research Council, 1943). In cases where the patient presented weakness on both sides, the stronger or more recently affected limb was selected..

3.1.3 Experimental Setup

All participants were in a comfortable semi-reclined position and fully relaxed. The elbow of the participant was extended and supported by a pillow. The leg was supported under the knee. The tested nerves and sites were the median nerve at the wrist level and the common fibular nerve at the knee level. EMG was recorded from the APB muscle and TA muscle. The skin areas of recording sites and stimulation sites were prepared using abrasive paper and alcohol wipes to reduce impedance. The active recording electrode (E1) was placed over the muscle belly and the reference electrode (E2) over the tendon of insertion of the tested muscle. The placement of E1 was optimized to record the muscle's largest response to supramaximal stimulation. Two Ag/AgCl non-polarizable stimulating electrodes were placed over the nerve after manually mapping the best stimulation site using the handheld stimulator; i.e. the location that induced the largest muscle contraction with the smallest stimulation intensity. The cathode

was placed distally over the mapped stimulation spot, approximately 3-4cm above the wrist crease for the median nerve and around the fibular head for the common fibular nerve. The anode was proximal and slightly lateral to the cathode to keep the anode away from the nerve. The ground electrode was positioned on the dorsum of the hand or the tibia. A temperature sensor was placed near the stimulating cathode and the skin temperature was kept between 32-34 °C during the recording time using a passive heating pad if necessary.

The stimulating electrodes were connected to a Digitimer DS5 stimulator controlled by the stimulation program (QtracS) in Qtrac software (© UCL Institute of Neurology, London, UK, available from Digitimer Ltd at www.Digitimer.com). Square wave pulses from the stimulator were delivered via the stimulating electrodes placed near the wrist or knee of the participant, and the EMG signals from the recording electrodes were directed to a Digitimer D440 amplifier. After amplification and bandpass filtering (gain 300-500, filter 3 - 3000 Hz), the signals passed through the Hum Bug to filter out 60Hz frequencies in real-time. The final signals were processed by the data acquisition board (National Instruments USB-6251; sampling frequency: 10 kHz) which can convert the electrical signals into digital information that can be read by the computer and the Qtrac software.

3.1.4 Nerve excitability tests

All the excitability tests were performed with Qtrac software using the TROND protocol (Kiernan et al., 2000). All the 32 indices retrieved from a NET can be analyzed and plotted offline by the plotting program (QTracP) in QTrac (see Appendix, Table 2).

3.2 Statistical analysis

3.2.1 Missing data

We observed a notably high rate of missing data for the 2ms refractoriness measurement in both the median and common fibular nerves. This can be attributed to the interaction between the interstimulus interval and the strength of the test stimulus. In some cases, the stimulus intensity exceeded the stimulator's maximum output (beyond 100%) before the interval reached 2 or 2.5 ms, leading to the absence of data points. Additionally, we identified missingness in several other indices (as discussed in Chapter 4.1). The missing values were due to individual physiological variations within the nerve that might or might not be captured by other measured indices within the NET, making the normative NET data potentially Missing Not At Random.

In order to get complete datasets from the available data without case deletion (which would cause the sample size to decrease from 201 to 137), we used imputation methods to fill in the missing data. Mean imputation was first explored. However, the relationships between the imputed variables and other variables may not be preserved in mean imputation and it is problematic for our correlation studies. Furthermore, with the unequal missing rates for different variables that we observed in our dataset (Table 4.2), the mean imputation method may cause inconsistent bias (Kang, 2013).

To overcome these limitations, we adopted the multiple imputation (MI) method, which accounts for the variability and uncertainty of the imputed data and facilitates the generation of valid statistical inferences (Kang, 2013; Little & Rubin, 2002). Multiple machine learning algorithms have been developed based on the concepts of different imputation methods. Among the 10 algorithms examined by Bell (2019), an iterating cascading autoencoder demonstrated the best performance across all sample sizes. This algorithm was tailored and optimized (MATLAB,

(The MathWorks Inc., 2022)) to suit the characteristics of the normative NET dataset, and used

to impute missing data within the arm and leg datasets from healthy controls.

3.2.2 Correlation Analyses

R Statistical Software (version 4.2.3; R Core Team, 2023) was used for correlation

analyses with the complete data sets. Before conducting the correlation analyses, the data were

checked for normality and outliers. Pearson's correlation coefficient (r) was used to determine the

strength and direction of the linear relationship between continuous variables. Correlation

matrices were calculated and plotted using the sjplot (Lüdecke, 2023), psych (Revelle, 2023),

and corrplot (Wei & Simko, 2021) packages, relating the 32 values of NET in the median nerve,

common fibular nerve, and between the two nerves. ppcor package (Kim, 2015) was used to do

the partial correlation analysis between the same indices of the two nerves. The partial

correlation analysis used age as a covariate to remove a potential confounder variable, allowing

for a clearer examination of the underlying association between the nerve excitability variables.

The significance level (α) was set *a priori* at 0.05. Additionally, the strength of the correlations

was assessed using established guidelines, for absolute values of correlation coefficients, $r<0.1$ is

regarded as negligible, $0.1 \leq r < 0.4$ as weak, $0.4 \leq r < 0.7$ as moderate, $0.7 \leq r < 0.9$ as strong, and r

≥ 0.9 as very strong relationship (Schober et al., 2018). The non-parametric Wilcoxon rank-sum

test in SPSS (version 22) was used to examine whether the NET relationships are different

between the two nerves since the correlation values were not normally distributed.

3.2.3 Exploratory factor analysis (EFA)

EFA was performed separately for the median nerve and common fibular nerve datasets

using the "fa" function from the "psych" package in R (version 4.2.3). The results were

visualized using the "ggplot2" package. During the process, a sequence of well-considered

methodological choices were made at each decision point, aiming to select the most suitable ones based on empirical evidence and best practices. The R code example for conducting an EFA can be found in the Appendix.

Index selection. Prior to conducting the EFA, an index selection process was implemented to address issues of multicollinearity. Initially, the correlation matrix was examined to identify highly correlated indices with a correlation coefficient above 0.90, indicating potential multicollinearity. To mitigate this, a stepwise index selection method was employed, where one index from each highly correlated pair was systematically removed from the analysis based on their theoretical relevance and measurement properties (Chapter 4.4.1). The Kaiser-Meyer-Olkin (KMO) measure of sampling adequacy (MSA) was utilized to assess the factorability of the data. Indices with a low MSA below 0.5 were systematically removed from the analysis to ensure the inclusion of indices that exhibited satisfactory sampling adequacy. By implementing this selection process, we aimed to enhance the reliability and validity of the subsequent factor analysis outcomes.

Bartlett's Test of Sphericity was then performed to assess the appropriateness of conducting factor analysis on the retained dataset. It examines whether the correlation matrix of the variables differs significantly from an identity matrix (no underlying factor structure).

The univariate and multivariate normality of the retained indices were examined by probability plots (such as Q-Q plot and P-P plot) and statistical measures (such as the skewness and kurtosis). A remedy approach should be employed if normality is severely violated (e.g. skewness > 2; kurtosis >7; West et al., 1995).

Factor extraction. To identify a set of factors that explain the common variance among the measured indices, the maximum likelihood (ML) method was used to extract factors. This

method is preferred when the distribution of the measured variables meets the assumptions of normality, as it provides additional information such as model fit indices (Fabrigar et al., 1999).

Once the factors are extracted, the next step is to determine the number of factors to retain in the analysis. Several methods were employed. Firstly, Kaiser's criterion was applied, which suggests retaining factors with eigenvalues greater than one as they explain a significant amount of variance in the observed variables (Kaiser, 1960). Additionally, the scree test and parallel analysis were conducted to further evaluate the number of factors to retain. Cattell's optimal coordinates, also known as Cattell's scree test, involves plotting the eigenvalues in descending order and retaining the factors before the "elbow" in the plot (Cattell, 1966). Horn's parallel analysis is based on comparing the observed eigenvalues to the eigenvalues obtained from simulated random data sets with the same sample size and the number of variables (Horn, 1965). The retained factors capture the underlying structure and explain the significant variance in the dataset beyond what can be attributed to chance.

Factor rotation. By applying rotation methods, factor analysis modifies the pattern of factor loadings to yield more meaningful and understandable structures. There are two primary types of factor rotation: orthogonal and oblique. Orthogonal rotations assume factors are uncorrelated and are suitable for uncorrelated factors. Oblique rotations allow for correlated factors and are preferable when factors are expected to be correlated (Costello & Osborne, 2005). Both methods were examined. The factor structures and fit indices were evaluated to determine the optimal fit. Fit indices, including Relative (incremental) fit measures, such as the Tucker-Lewis Index of factoring reliability (TLI) and Absolute fit measures, such as Root Mean Square Error of Approximation (RMSEA) were compared. For over seven observed variables, a TLI value exceeding 0.9 was indicative of a good fit. For RMSEA, values of ≤ 0.01 indicated

excellent fit, ≤ 0.05 good fit, ≤ 0.08 moderate fit, and values ≥ 0.10 suggested poor fit (Hu & Bentler, 1999). The obtained rotated factor solution was subsequently employed for further interpretation and analysis.

Factor loadings, representing the relationships between each variable and the identified factors, were assessed for significance. They can range from -1 to 1. A positive factor loading indicates a positive correlation between the observed variable and the latent factor, while a negative factor loading indicates a negative correlation. Higher absolute factor loadings suggest a stronger connection between the variable and the factor while lower factor loadings suggest a weaker connection. Loadings greater than 0.40 were considered significant and were used to interpret the factors (Stevens, 1992). The interpretation of the factors was based on the pattern of high loadings and the content of the indices that contributed most strongly to each factor. More stringent cut-offs are 0.32 (poor), 0.45 (fair), 0.55 (good), 0.63 (very good), or 0.71 (excellent) (Comrey & Lee, 1992; Tabachnick & Fidell, 2007).

Factor scores. The default regression method in R was used to calculate the factor scores. To ensure a meaningful comparison, the datasets from controls and patients, such as the median nerve datasets, were combined and scaled together before computing the factor scores. This guarantees that the factor scores are derived from a consistent scaling across both groups.

3.2.4 Covariate Adjustments and Group Comparison

The effect of age and sex on the factor scores in the healthy control group was examined using two-way ANOVA tests in SPSS Version 23.0 (IBM Corp, 2015). Age was categorized into three groups: young (<40 y.o.), middle-aged (40-59 y.o.), and old (≥60 y.o.), in accordance with

prior literature on age-related variations in NET (McHugh et al., 2011). Sex was categorized as male and female. Post-hoc tests and p-value adjustments, using the Bonferroni method, were performed to identify specific group differences. The Bonferroni method provides control over the family-wise error rate (FWER), which is the probability of making at least one Type I error (false positive) in a set of multiple hypothesis tests. The effect size for the ANOVA test, Partial Eta Squared (η^2), was reported. $\eta^2 = 0.01$ indicates a small effect, $\eta^2 = 0.06$ indicates a medium effect, $\eta^2 = 0.14$ indicates a large effect (Cohen, 1969).

Furthermore, ANCOVA tests were conducted to examine the differences in factor scores for each factor in the median and common fibular nerves between older controls (age ≥ 40 y.o.) and people with ALS, while accounting for the covariates of age and sex to control for potential confounding effects. Due to the ALS group's sample size being less than 20, Hedge's g was calculated to determine the effect size (Hedges, 1981). A Hedge's g value of 0.2 is considered a small effect, 0.5 a medium effect, and 0.8 or above a large effect (Cohen, 1992).

Chapter 4: Results

4.1 Demographic Characteristics

A total of 201 healthy participants (91 males and 110 females) were included in this study, with data collected from the CTN Lab between May 2015 and September 2022. These participants underwent successful NET for both their upper and lower limbs. The data for the 15 people diagnosed with ALS was collected from July 2021 to February 2023. Successful NET recordings were made in 11 median nerves and 12 common fibular nerves in these patients. To address the substantial age difference between the control and ALS groups, we created a subgroup of controls with comparable age ($\geq$40 y.o.) to the ALS sample, referred to as the "older controls." Table 4.1 and Figure 4.1 illustrate the distribution of age and sex among the healthy control group and the ALS group. Detailed information on the people with ALS is provided in Appendix Table 3.

Table 4.1 Characteristics of the healthy control group and ALS group

Group	n	Age (y), mean±SD	Sex
Control	201	38.5±17.1	91 male, 110 female
Older Control	84	56.3±10.46	36 male, 48 female
ALS	15	61.9±7.98	9 male, 6 female
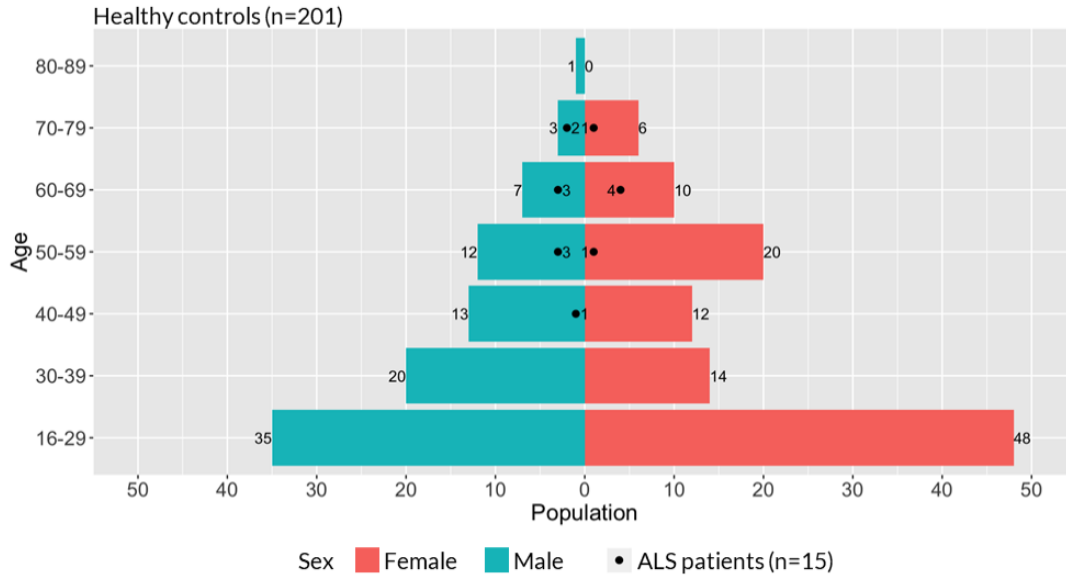
Figure 4.1 Age-sex distribution for healthy controls and people diagnosed with ALS. The y-axis represents the age range, while the x-axis represents the population. The black dots indicate the number of people with ALS.

4.2 Missing Values

Analysis of the data revealed certain patterns of missing values in the two nerves, as summarized in Table 4.2. Specifically, in healthy controls, the hyperpolarization I/V slope exhibited the highest rate of missing values in the common fibular nerve. Similarly, refractoriness at 2 ms (%) displayed a comparable rate of missing values in both the median and common fibular nerve.

For the ALS group, there is a slightly higher missing rate for hyperpolarization I/V slope in the median nerve, but no missing values for refractoriness at 2 or 2.5ms. However, over half of the patients have missing values in refractoriness at 2ms in the common fibular nerve.

Table 4.2 Missing Counts and Rates of the NET indices that have missing data in Median Nerve and Common Fibular Nerve.

Indices	Missing Count (Percent)			
	Median Nerve		**Common Fibular Nerve**	
	Controls	**ALS**	**Controls**	**ALS**
TEh(90–100ms)	—	—	1 (0.5%)	—
TEh(slope 101-140ms)	—	—	1 (0.5%)	—
TEh(overshoot)	1 (0.5%)	—	3 (1.5%)	—
Resting I/V slope	—	—	2 (1.0%)	—
Minimum I/V slope	—	—	1 (0.5%)	—
Hyperpol. I/V slope	1 (0.5%)	3 (25%)	34 (16.9%)	2 (16.7%)
Refractoriness at 2 ms	29 (14.4%)	—	31 (15.4%)	7 (58.3%)
Refractoriness at 2.5ms	7 (3.5%)	—	1 (0.5%)	1 (8.3%)

4.3 Correlations in Nerve Excitability Indices

4.3.1 NET indices within a nerve are not independent

The correlation matrices in the median and common fibular nerve are shown in Figure 4.2 and 4.3, respectively. The correlation coefficients and their corresponding p-values for the median and common fibular nerves are presented in Supplementary Tables 1 and 2. There are 496 correlation pairs between the 32 NET indices in a single nerve.

Although the patterns of the matrices (covariance structure) appear similar between the two limbs, the Wilcoxon rank sum test revealed that the correlations between the indices in the common fibular nerve are significantly different compared to those in the median nerve (314 positive ranks, $Z = -7.281$, $p < 0.001$). The numbers of correlations in each correlation strength group (cf. Schober et al., 2018) for the two tests are listed in Table 4.3.
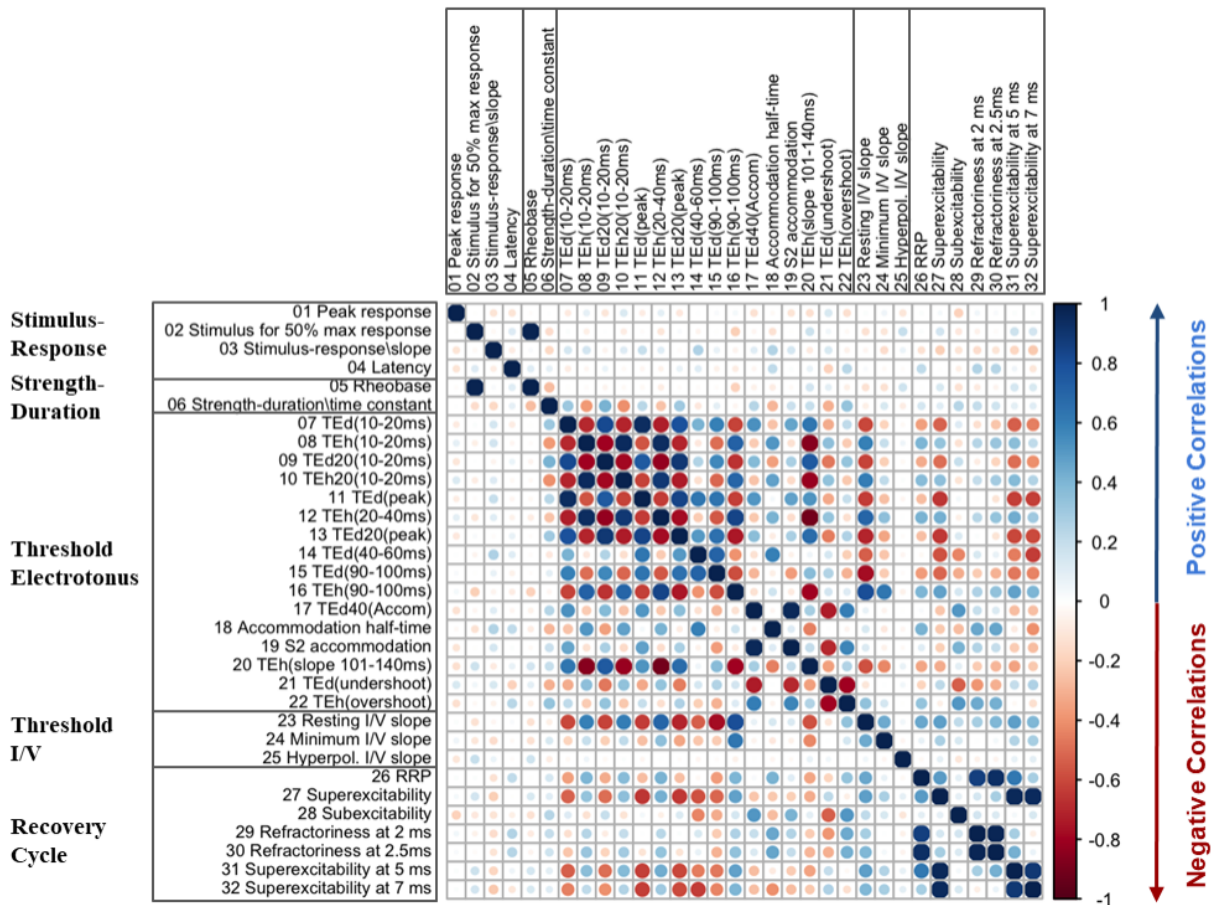
Figure 4.2 Correlation matrix of NET indices in the median nerve using Pearson correlation test. Blue dots indicate positive correlations and red dots indicate negative correlations. The darker the colour, the greater the *r*-value. The size of the circle represents the inverse of the p-value. The larger the circle, the smaller the p-value. The matrix is symmetric. The diagonal cells of the matrix show the correlation of each index with itself, which is always equal to 1. The indices listed within the same box belong to one subtest, as indicated on the left side. Most strong correlations were within the same subtests, particularly during threshold electrotonus. Surprising correlations were observed between different phases and conditioning currents in threshold electrotonus (#8 with #16, #21 with #22) and in the recovery cycle (#26 with #27, #31 and#32). Additionally, indices in threshold electrotonus, such as #7–#14, exhibited a strong association with resting I/V slope (#23). They also exhibited a moderate correlation with superexcitability (#27).
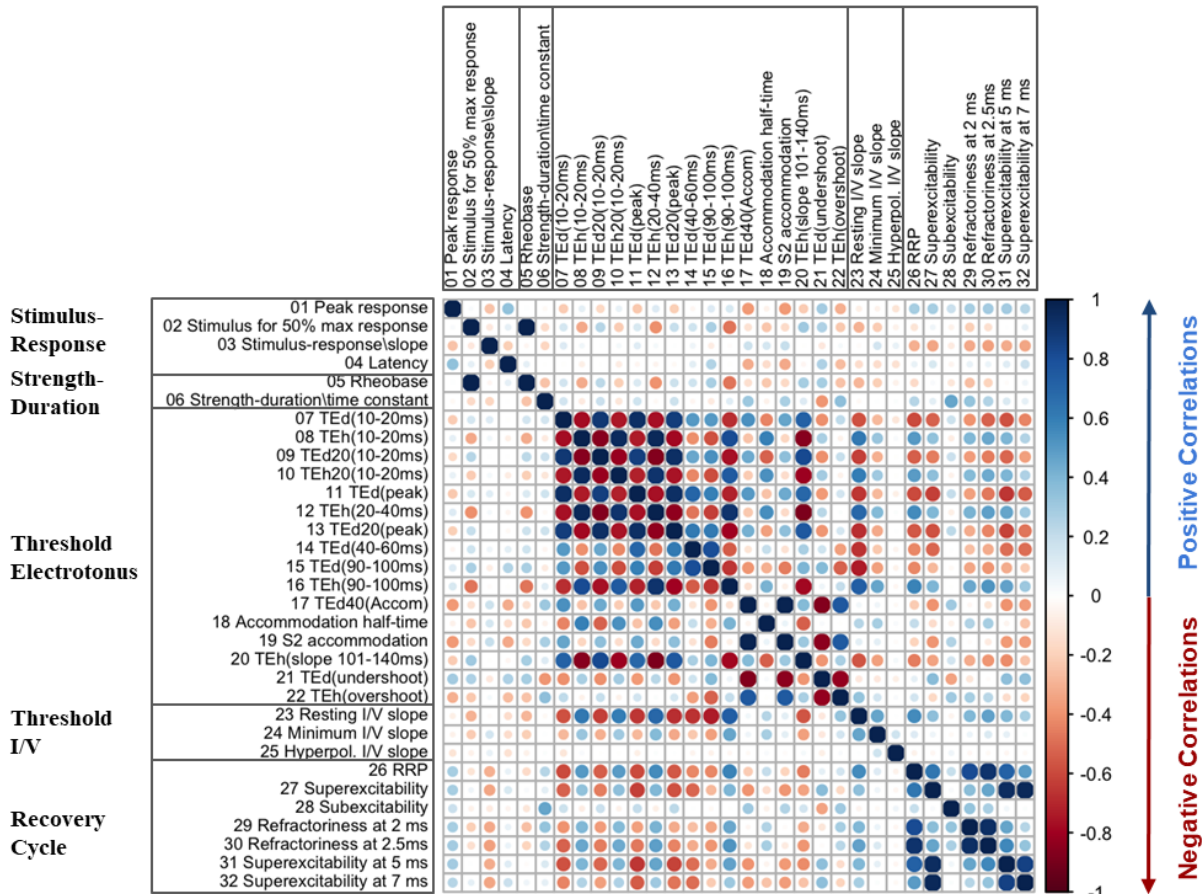
Figure 4.3 Correlation matrix of NET indices in the common fibular nerve using Pearson correlation test. Blue dots reflect positive correlations and red dots indicate negative correlations. The darker the colour, the greater the *r*-value. The size of the circle represents the inverse of the p-value. The larger the circle, the smaller the p-value. The matrix is symmetric. The diagonal cells of the matrix show the correlation of each index with itself, which is always equal to 1. The indices listed within the same box belong to one subtest, as indicated on the left side. The overall covariance structure in the common fibular nerve is similar to that observed in the median nerve, but with many of the correlations being stronger in the common fibular nerve.

Table 4.3 Counts and rates of correlations in the median nerve and common fibular nerve with Pearson correlation test.

Correlation strength	Median Nerve (%)	Common Fibular Nerve (%)
Very strong	10 (2.0)	13 (2.6)
Strong	31 (6.3)	39 (7.9)
Moderate	88 (17.7)	98 (19.8)

Note: Correlation strength: very strong: $r \geq 0.9$; strong: $0.7 \leq r < 0.9$; moderate: $0.4 \leq r < 0.7$ (Schober et al., 2018).

Among the correlations that met or exceeded a strong strength (Table 4.3), over 80% of correlations occurred between indices from the same TROND subtest (within-subtest), especially during threshold electrotonus. In the median nerve, 36 out of 41, and in the common fibular nerve, 49 out of 52 very strong and strong correlations are within subtests. Many of these high correlations are expected based on the nature of the measurement (e.g. indices at the same time point in depolarizing and hyperpolarizing threshold electrotonus), but some were unexpected: such as indices from nonadjacent phases: TEh(10–20ms) & TEh(90–100ms) ($r = 0.73$ & 0.82 for median & common fibular nerve), indices in two conditioning currents: TEd20(10–20ms) & TEh(slope 101–140ms) ($r = 0.76$ & 0.82), TEd(undershoot) & TEh(overshoot) ($r = -0.79$ & -0.821). In the recovery cycle, RRP was moderately correlated with superexcitability indices (including superexcitability at peak, 5ms and 7ms) in both nerves (r ranging from 0.49 to 0.73).

For between–subtest correlations, surprisingly strong correlations were observed between some indices from the threshold electrotonus and the threshold I/V subtest. In particular, both TEd(90–100ms) and TEh(90–100ms) were strongly correlated with resting I//V slope in both nerves (absolute r ranging from 0.7 to 0.81). Some moderate correlations between subtests are also consistent in both nerves. Superexcitability showed moderate negative correlations with depolarizing threshold electrotonus indices such as TEd(10–20ms), TEd(peak), TEd(40–60ms)

and TEd(90–100ms) (*r* ranging from -0.46 to -0.65). There was a positive correlation between superexcitability with hyperpolarizing threshold electrotonus at 90–100ms in both nerves (*r* = 0.48 & 0.41).

To sum up, the NET indices within a nerve are not independent of each other and the correlation analysis showed differences between the two nerves, with stronger correlations in the common fibular nerve.

4.3.2 Most NET indices are independent between nerves of the upper and lower limb

There are a total of 1024 correlation pairs between the 32 NET indices of the two nerves (Figure 4.4). The on-diagonal correlations (total of 32) were a focus to determine the relationship between the same excitability index in the upper and lower limbs. In total, 24 out of the 32 on-diagonal correlations had an *r* ≥ 0.3 (medium effect size, (Cohen, 1992)) (Table 4.4); they were all positive relationships. Partial correlation analyses revealed that, after accounting for age as a covariate, 23 out of the 24 correlations were less than 0.3, except for TEh(overshoot) (from 0.46 to 0.33). The correlation for the minimum I/V slope became slightly stronger (from 0.35 to 0.42) (Table 4.4).

Table 4.4 On-Diagonal Correlations (corresponding indices of the median and common fibular nerve) with Pearson $r \geq 0.3$ and their partial correlations after controlling for age.

Index	*r*(partial *r*)	Index	*r*(partial *r*)	Index	*r*(partial *r*)
Superexcitability	0.55(0.23)	Superexcitability at 7 ms	0.49(0.24)	SDTC	0.38(0.26)
Superexcitability at 5 ms	0.54(0.22)	TEh(90–100ms)	0.48(0.28)	TEd(undershoot)	0.38(-0.21)
TEd20(peak)	0.51(-0.03)	RRP	0.47(0.10)	TEd(10–20ms)	0.37(-0.04)
TEd(90–100ms)	0.5(-0.12)	Resting I/V slope	0.47(0.13)	Refractoriness at 2 ms	0.37(0.06)
		TEh(overshoot)	0.46(**0.33**)	TEh(20–40ms)	0.36(0.04)
		TEd40(Accom)	0.45(0.02)	TEh(slope 101-140ms)	0.35(0.02)
		TEd(peak)	0.44(-0.14)	Minimum I/V slope	0.35(**0.42**)
		Peak response	0.44(-0.15)	TEh(10–20ms)	0.34(-0.08)
		Refractoriness at 2.5ms	0.44(0.05)	TEd20(10–20ms)	0.34(0.09)
		S2 accommodation	0.43(-0.03)		
		TEd(40–60ms)	0.4(-0.27)		

Note: The correlations have been grouped into three columns based on the magnitude of the original Pearson coefficients *r*: the first column includes *r* values above 0.5, the second column includes *r* values between 0.4 and 0.5, and the third column contains *r* values between 0.3 and 0.4. The partial correlations higher than 0.3 are bolded. SDTC: Strength duration time constant.
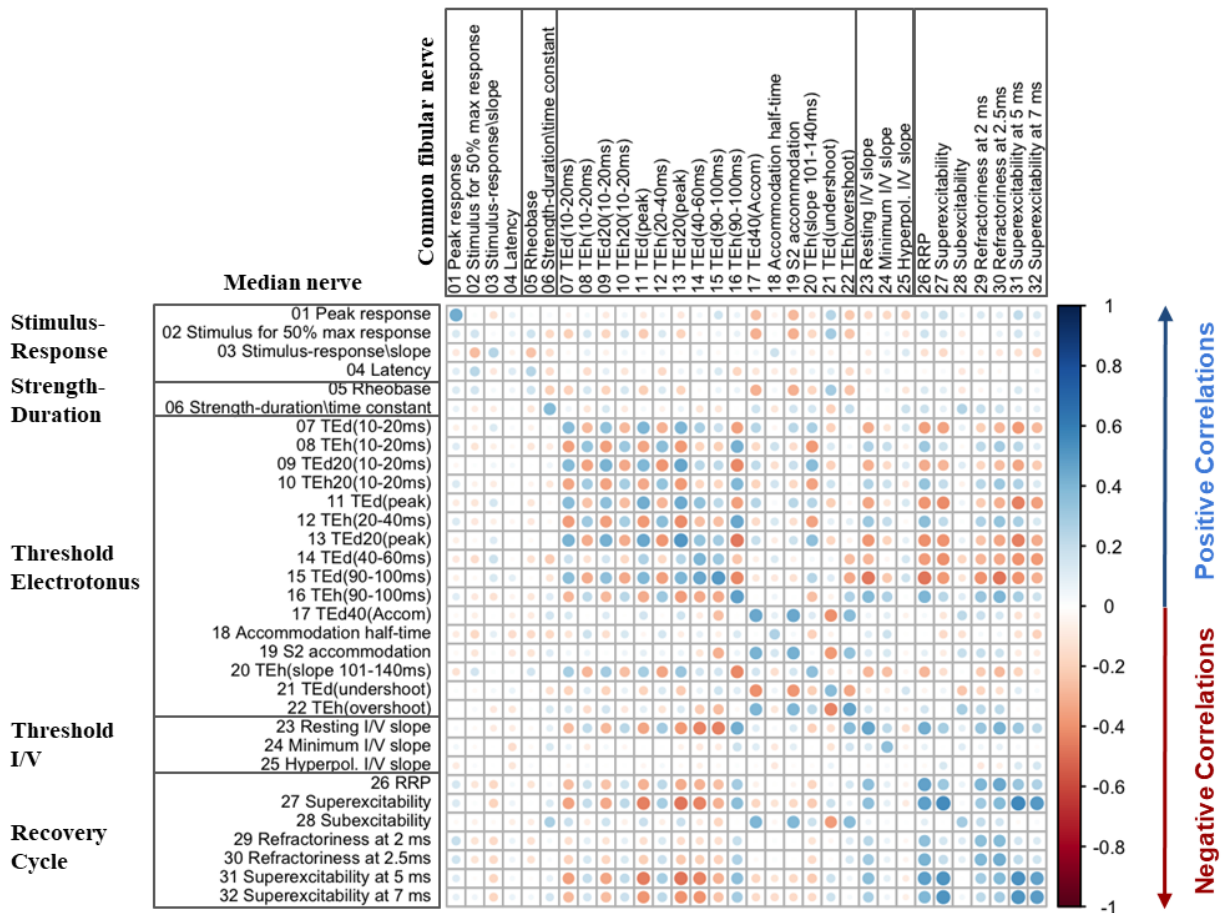
Figure 4.4 Correlation matrix of NET indices between median and common fibular nerves using Pearson correlation test. Blue dots reflect positive correlations and red dots indicate negative correlations. The darker the colour, the greater the relationship. The size of the circle represents the inverse of the p-value. The larger the circle, the smaller the p-value. The matrix is not symmetric, meaning that the correlation between index A and index B is different from the correlation between index B and index A. The indices presented on the left side pertain to the median nerve, while the indices on the top side pertain to the common fibular nerve. The indices listed within the same box belong to one subtest, as indicated on the left side. The correlations between the same indices of the median and common fibular nerve are the on-diagonal dots. They are all weak to moderate positive correlations.

In summary, most of the correlations between the same indices in the median and common fibular nerve were below a threshold of $r \geq 0.3$ after controlling for age, except for the minimum I/V slope and TEh(overshoot). This indicates a weak correlation, or independence, of the same excitability index in the upper and lower limbs.

4.4 EFA Results

Given the presence of within-nerve correlations in both the median and common fibular nerves, EFA was conducted to identify latent factors within the excitability indices of a single nerve. The distinct correlation patterns within each nerve suggest that the underlying structures differ, leading to separate EFA analyses for each nerve.

4.4.1 16 indices retained for the EFA after index selection

During the index selection process, we identified and removed 10 redundant indices from the median nerve dataset. The selection was based on the following principle: prioritizing indices that are commonly reported in nerve excitability studies and provide generalizable information. For instance, we prioritized rheobase over stimulus for 50% max response, and superexcitability over superexcitability at 5ms and 7ms. Decisions were also influenced by a systematic review and meta-analysis that evaluated which indices consistently differentiated between people diagnosed with ALS and healthy controls (Lugg et al., 2022). We also examined the pairs of indices with a correlation coefficient between 0.8 and 0.9, and further identified and eliminated redundant indices. The decision process for the median nerve is illustrated in Figure 4.5. Six indices were removed for a low measure of sampling adequacy (MSA<0.5): hyperpolarizing I/V slope, rheobase, S2 accommodation, peak response, accommodation half-time, and latency. None of these were within the seven indices that can differentiate people diagnosed with ALS and healthy controls (Lugg et al., 2022).

r=0.99 — Stimulus for 50% max response / Rheobase | TEh(10-20ms) / TEh20(10-20ms) — 0.95

0.97 — Refractoriness at 2 ms / Refractoriness at 2.5 ms | TEh(10-20ms) / TEh(20-40ms) — 0.95

0.97 — Superexcitability / Superexcitability at 5 ms | TEd(10-20ms) / TEd(peak) — 0.95

0.96 — TEd40(Accom) / S2 accommodation | TEd20(10-20ms) / TEd20(peak) — 0.90

0.96 — Superexcitability / Superexcitability at 7 ms | TEd(10-20ms) / TEd20(10-20ms) — 0.82
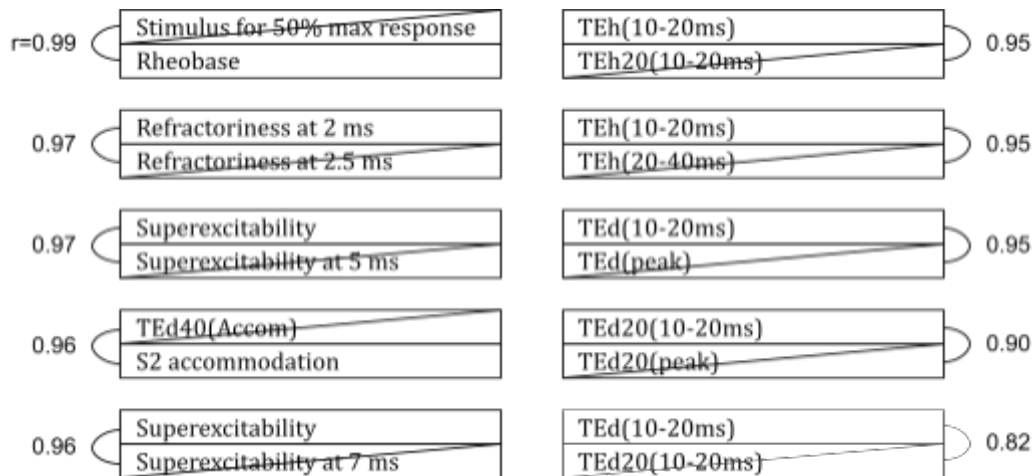
Figure 4.5 Index selection for highly correlated pairs in the median nerve. Pairs with *r*-values >0.80 were identified that had potentially co-dependent or redundant information and one was excluded (crossed out). 10 redundant indices were removed.

A total of 16 indices remained for the conduct of EFA in the median nerve. The overall MSA value obtained was 0.74. The cutoff value of KMO $\geq$ 0.60, as recommended by Kaiser (1974), was employed to determine the factorability of the sample.

The index selection procedure in the common fibular nerve dataset followed a similar approach as in the median nerve. To ensure consistency between the two datasets, the same indices were initially retained. Furthermore, when considering the factor structures, a decision was made to choose a single index from the pair TEd(10–20ms) and TEd(peak). In this case, TEd(peak) was selected for the common fibular nerve dataset due to its simpler and more interpretable structure. The overall MSA value obtained was 0.78.

Bartlett's test (p-value < 0.001) in both the median nerve and the common fibular nerve indicated that the two NET datasets met the criteria for conducting a factor analysis. And the 16 indices retained for both nerves did not exhibit severe non-normality.

4.4.2 EFA generated a five-factor model in median nerve NET

There were five factors with initial eigenvalues higher than 1.0 in the common fibular nerve NET dataset. The scree test (scree plot in Figure 4.6) and parallel analysis (Figure 4.7) consistently supported the selection of the optimal number of factors to retain.
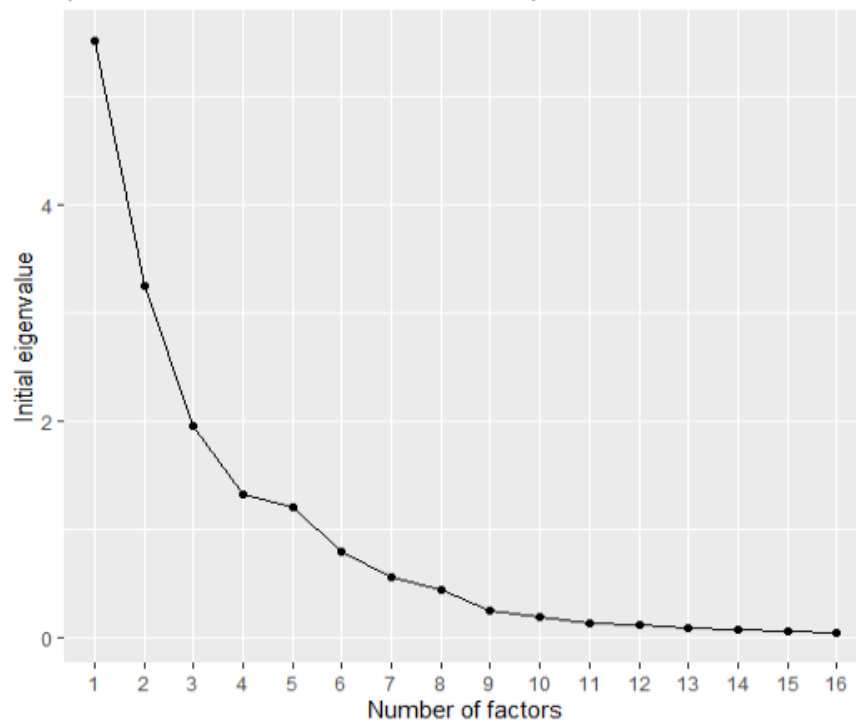
Figure 4.6 Scree plot based on the unreduced correlation matrix for the 16 NET indices in the median nerve. The x-axis represents the number of factors in the dataset, while the y-axis represents the corresponding eigenvalues. Each point on the plot represents an eigenvalue derived from principal components analysis. The "elbow" point occurs after the fifth factor on the plot, indicating that retaining five factors captures the most significant variance in the data. Initial eigenvalues: 5.51616450, 3.25731545, 1.95497047, 1.32266372, and 1.20163365.
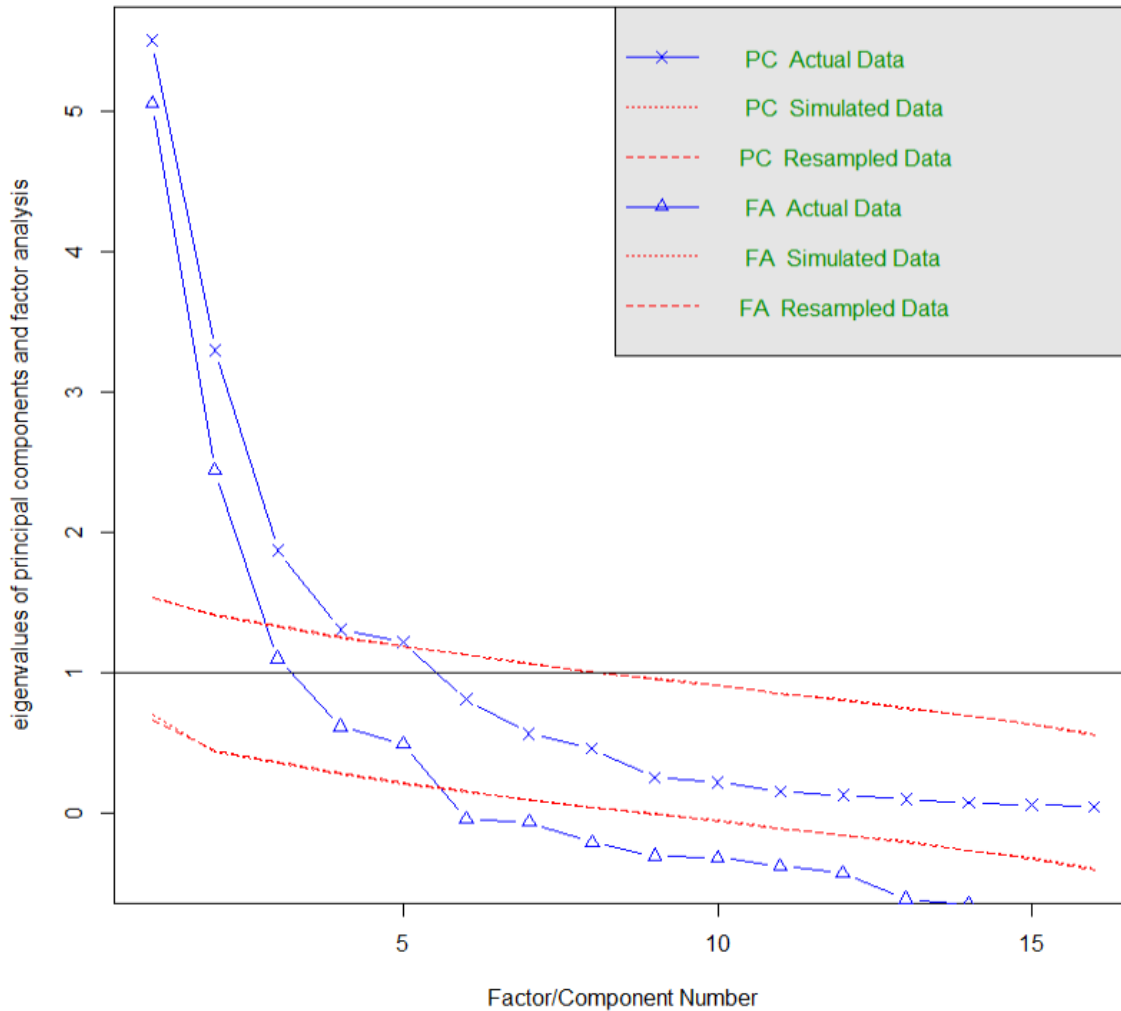
Figure 4.7 Parallel analysis scree plots for the 16 NET indices in the median nerve. The scree plot displays the eigenvalues for each factor obtained from the actual data in blue and the eigenvalues obtained from parallel analysis (using simulated random data) in red. The decision point for determining the number of factors to retain is where the blue line (actual data) intersects the red line (parallel analysis). The first five factors with eigenvalues above this intersection point are considered meaningful and retained, while factors below this point are considered insignificant and discarded. These five factors explain more variance in the data than what would be expected by chance in random data.
PC = principal components; FA = factor analysis.

Multiple models, such as four-factor and six-factor models, were tested and the model fit

indices were compared. In the six-factor model, regardless of the rotation method used, there

were one or more factors that had only one index loading on them, and two or more factors had

two indices loading on them. The fit indices for the four-factor model (Tucker Lewis Index (TLI) = 0.67, Root Mean Square Error of Approximation (RMSEA) index = 0.2 with the 90 % confidence intervals [0.18564 0.21607]) were not as good as the five-factor model (TLI = 0.84, RMSEA index = 0.14 with the 90 % CI [0.12235, 0.15726]) (TLI > 0.90 is considered as good fit, RMSEA ≥ 0.10 indicates poor fit, Hu & Bentler, 1999).

A comparison was also made between orthogonal and oblique rotation methods with the five-factor model. The fit indices for both models were found to be identical. While the oblique rotation did not lead to a significant enhancement in the relative model fit based on fit indices, it was preferred over the more parsimonious structure because the item loadings were better and more interpretable. The orthogonal (varimax) rotation had two factors with only two indices loading on them, one pair loading on one factor had a weak correlation (r = -0.17), making the factor unreliable (Yong & Pearce, 2013). The promax rotation method was selected, aiming to maximize the simplicity of the factor structure and produce uncorrelated factors with high loadings. At last, the five-factor model with the oblique (promax) rotation was chosen for the median nerve dataset (Figure 4.8).

The factor loadings for each index after oblique rotation are listed in <u>Appendix Table 4</u>. Loadings greater than 0.40 were considered significant. The five factors extracted from the analysis accounted for 75% of the total variance. The mean communalities of the 16 indices was 0.75. Based on the pattern of factor loadings and the content of the variables associated with each factor, the factors were interpreted as follows: M1: K_s and Na_p channels, M2:HCN channels, M3:nodal K_s channels, M4: Na channels and M5: passive electrical properties.

Figure 4.8 EFA model for the median nerve. The loadings of each index on their respective factors are shown on the lines. The factor correlations are shown on the right side of the factors. The variance explained by each factor is listed under them. The total variance explained by these five factors is 75%.

There were four correlated pairs observed among the five factors in the median nerve. Specifically, M1 exhibited a negative correlation with M2 ($r = -0.6$) and M4 ($r = -0.4$). A positive correlation was observed between M2 and M4 ($r = 0.4$), while M3 showed a positive correlation with M5 ($r = 0.4$).

4.4.3 EFA generated a four-factor model in common fibular nerve NET

There were four factors with initial eigenvalues higher than 1.0 in the common fibular

nerve NET dataset. The scree test (Figure 4.9) and parallel analysis (Figure 4.10), consistently

supported the decision to retain four factors as the optimal number.
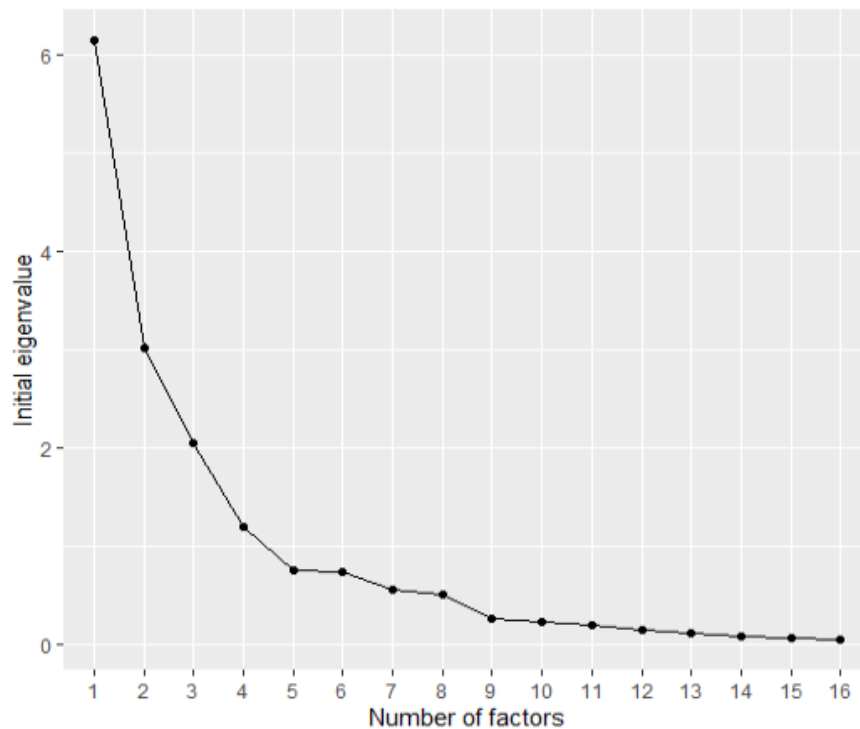
Figure 4.9 Scree plot based on the unreduced correlation matrix for the 16 NET indices in the common fibular nerve. The x-axis represents the number of factors in the dataset, while the y-axis represents the corresponding eigenvalues. Each point on the plot represents an eigenvalue derived from principal components analysis. The "elbow" point occurs after the fourth factor on the plot, indicating that retaining four factors captures the most significant variance in the data. Initial eigenvalues: 6.14468272, 3.00924927, 2.04537849, and 1.19034377.
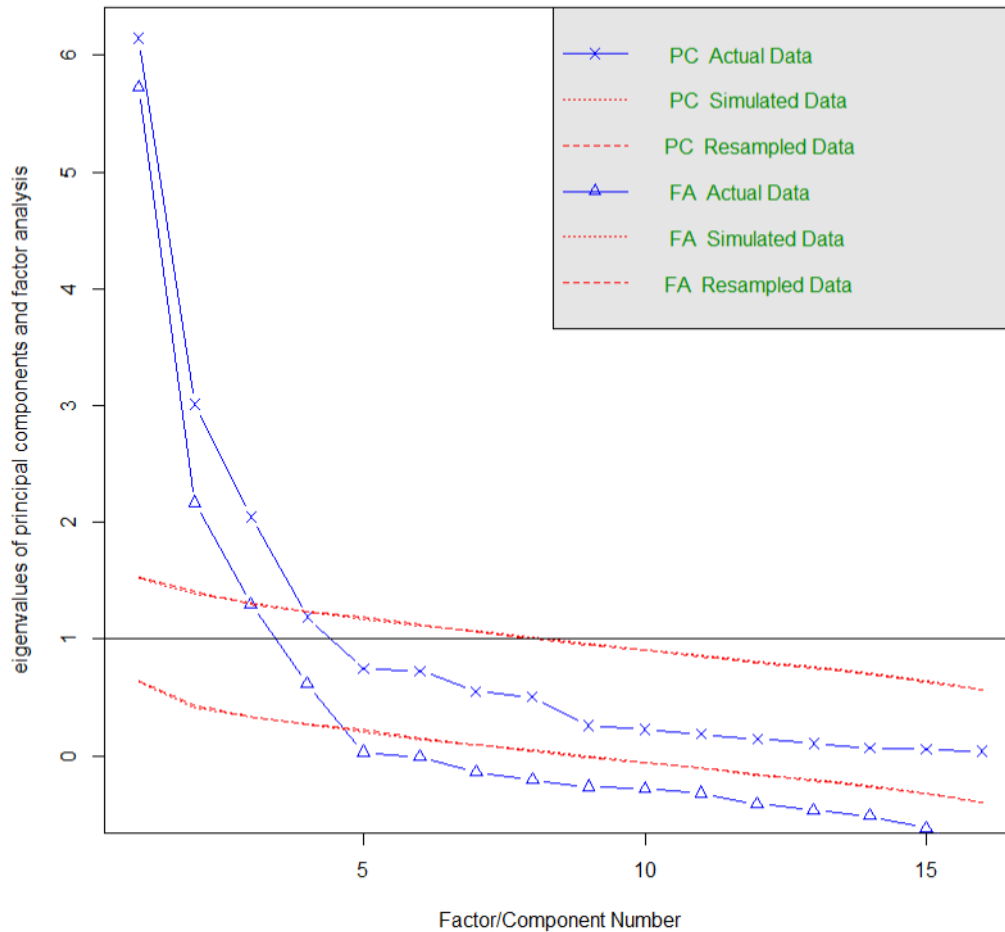
Figure 4.10 Parallel analysis scree plots for the 16 NET indices in the common fibular nerve. The scree plot displays the eigenvalues for each factor obtained from the actual data in blue and the eigenvalues obtained from parallel analysis (using simulated random data) in red. The decision point for determining the number of factors to retain is where the blue line (actual data) intersects the red line (parallel analysis). The first four factors with eigenvalues above this intersection point are considered meaningful and retained, while factors below this point are considered insignificant and discarded. These four factors explain more variance in the data than what would be expected by chance in random data.

PC = principal components; FA = factor analysis.

We also examined the three and five-factor model. The five-factor model had one factor with no index loading on it. The fit indices of the three-factor model (TLI = 0.63, RMSEA index = 0.21 with 90 % CI [0..198, 0.22559]) were not as good as the four-factor model (TLI = 0.83, RMSEA index = 0.14 with 90 % CI [0.12754, 0.15882]). The orthogonal (varimax) rotation showed one factor with only two indices loading on them, while the factors from the oblique (promax) rotation all had three or more indices loading on them. Thus, the four-factor model with oblique (promax) rotation has the most interpretability with fit indices. It was chosen for the common fibular nerve dataset (Figure 4.11).

The factor loadings for each index after oblique rotation were listed in Appendix Table 5. Loadings greater than .40 were shown in the same factor. The four factors extracted from the analysis accounted for 70% of the total variance. The mean communalities of the indices was 0.70. Based on the pattern of factor loadings and the content of the variables associated with each factor, the factors were interpreted as follows: CF1: HCN channels, CF2: nodal K_s channels, CF3: K_s and Na_p channels, and CF4: Na channels.

Regarding the correlations between factors, there was a negative correlation observed between CF1 and CF3 (r = -0.6).
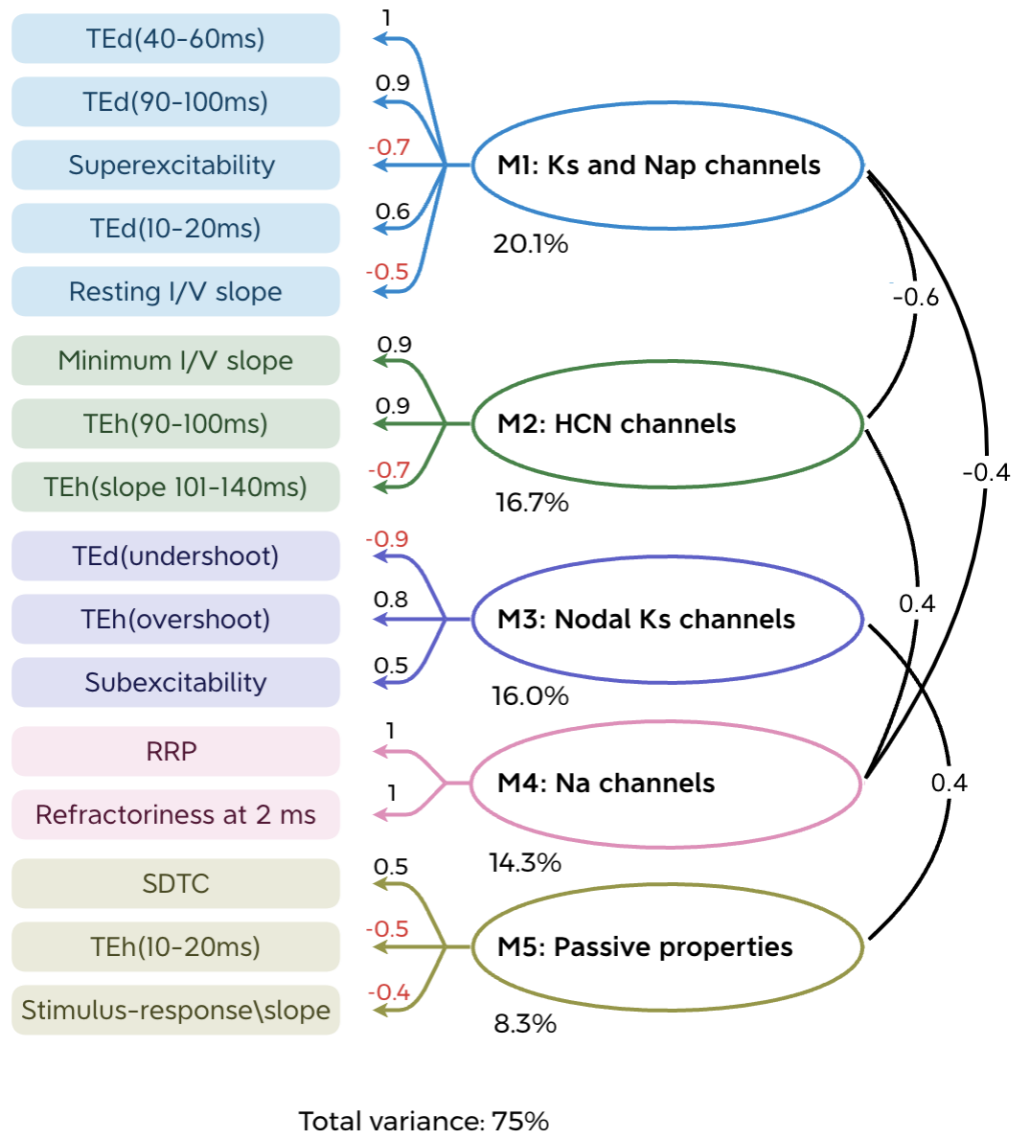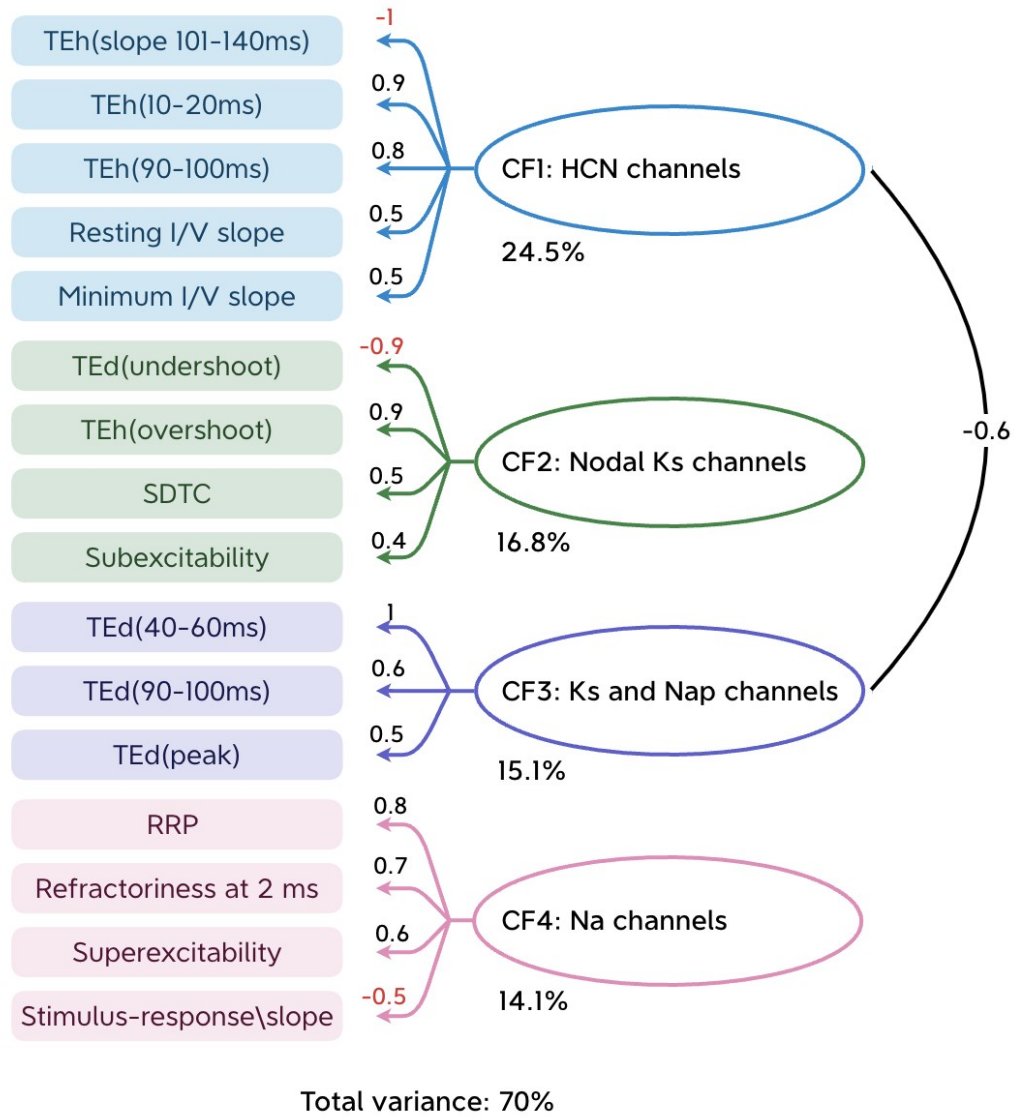
Figure 4.11 EFA model for the common fibular nerve. The loadings of each index on their respective factors are shown on the lines. The factor correlations are shown on the right side of the factors. The variance explained by each factor is listed under them. The total variance explained by these five factors is 70%.

4.5 Age and Sex Effects on Factor Scores in Normative NET Data

      After identifying the underlying factors and reducing the dimensionality of the NET from 30+ indices to 5 factors for the median nerve and 4 factors for the common fibular nerve, further analysis was conducted to examine the variations of these factors in relation to age and sex. The normative dataset was stratified into three age categories: young (<40 y.o. N = 117), middle-aged (40-59 y.o. N = 57), and old (≥60 y.o., N = 27). This stratification allowed for the investigation of potential age-related differences in the factor scores and their association with sex.

4.5.1 Both age and sex influence most of the Median nerve factor scores

      Data were normally distributed in all age-sex combination groups for M1, M2, M4 and M5, as assessed by Shapiro-Wilk's test (p > .05) or z scores of skewness and kurtosis (z within ±2.58), After visual examination of the data, it was determined that for M3, there was one outlier in middle age female group and one in old age female group (as assessed as being greater than 3 box-lengths from the edge of the box in a boxplot). After removing the outliers, the M3 factor scores were normally distributed in all groups, which provided evidence that the outliers were driving the deviations of normality. However, as the scores of the outlying participants reflected plausible values on the nerve tests, and due to the relatively small sample size, we chose to retain the outlier participants in the sample for the subsequent analyses.

      There was homogeneity of variances in all 5 median nerve EFA factors, as assessed by Levene's test for equality of variances (p > .05). Two-way ANOVA tests revealed no statistically significant age-by-sex interaction effects for any of the median nerve factors. However, there were statistically significant main effects of age on the M1 factor scores ($F(2, 195) = 3.336$, p = .038, partial η^2 = .033, small effect, Cohen, 1969), M2 factor scores ($F(2, 195) = 6.242$, p = .002, partial η^2 = .060, medium effect), M3 factor scores ($F(2, 195) = 7.893$, p = .001, partial η^2 = .075,

medium effect), and M5 factor scores ($F(2, 195) = 23.655$, $p < .001$, partial $\eta^2 = .195$, large effect). Post-hoc tests were then conducted to explore specific pairwise differences between the age groups for each factor score. The post hoc comparisons revealed that there were no significant differences in M1 factor scores between the age groups (Figure 4.12 A). In M2 factor scores (Figure 4.12 B), the middle age group had a significantly higher mean score of 0.554, 95% CI [0.174, 0.934], compared to the young age group ($p = .002$). Similarly, in M3 factor scores (Figure 4.12 C), the middle age group had a significantly higher mean score of 0.598, 95% CI [0.236, 0.960], compared to the young age group ($p < .001$). In M5 factor scores (Figure 4.12 E), the young age group had significantly lower mean scores compared to the other two groups, with mean differences of 0.813, 95% CI [0.478, 1.145], and 0.942, 95% CI [0.501, 1.383], both $p < 0.001$. There was no statistically significant age-related effect observed in the M4 factor, and the effect size was trivial.

Regarding sex differences, females showed significantly higher scores than males in M1 ($F(1,195) = 6.245$, $p = 0.013$, partial $\eta^2 = .031$, small effect) and M3 ($F(1,195) = 5.9553$, $p = 0.030$, partial $\eta^2 = .060$, medium effect) (Figure 4.11 A&C). Conversely, males had higher scores than females in M4 ($F(1,195) = 7.146$, $p = 0.008$, partial $\eta^2 = .035$, small effect) (Figure 4.12 D). No significant effects of sex were found on M2 and M5 scores, with trivial effect sizes.

In summary, the differences in the median nerve factor scores are primarily observed between the young and the two older groups, while the sex differences remain relatively consistent across all age groups.

Figure 4.12 Line plots depicting the effects of age and sex on the factor scores in the median nerve. Age was categorized into three groups: <40 years (young), 40-59 years (middle-aged), and ≥60 years (old). A. M1 factor scores in the median nerve exhibited both age and sex effects, with a significant difference observed only in sex. B. M2 factor scores showed a significant age effect between the young and middle-aged groups. C. M3 factor scores displayed significant effects of both age and sex. The age effect was significant between the young and middle-aged groups. D. M4 factor scores demonstrated a significant sex effect. E. Significant age effects were observed between the young and the two older groups on M5 factor scores. Female factor scores are represented by the red line, while male factor scores are represented by the blue line. Significance level: * p < 0.05, ** p < 0.01, *** p < 0.001.

4.5.2 Age and sex have small effects on some of the common fibular nerve factor scores

Data were normally distributed in all age-sex combination groups for CF1, CF3, and CF4, as assessed by Shapiro-Wilk's test ($p > .05$) or z scores of skewness and kurtosis (z within ±2.58). For CF2, after visually examining the data, one outlier in the old-age female group had driven the deviation of normality. We retained that for further analysis. The assumption of homogeneity of variances was not severely violated in all factor scores in the common fibular nerve, as assessed by Levene's test and standard deviation comparison. There was a statistically significant interaction between sex and age group for the CF2 factor score in the common fibular nerve ($F(2, 195) = 3.261$, $p = 0.04$). No significant interactions were observed for the other common fibular nerve factors. Age showed significant main effects on CF1 factor scores ($F(2, 195) = 5.752$, $p = 0.004$, partial $\eta^2 = .055$, small effect), CF2 factor scores ($F(2, 195) = 5.461$, $p = 0.005$, partial $\eta^2 = .053$, small effect), and CF4 factor scores ($F(2, 195) = 4.523$, $p = 0.012$, partial $\eta^2 = .044$, small effect) in the four factors of the common fibular nerve (Figure 4.13 A, B & C). Post-hoc tests revealed that participants in the young age group had a significantly higher mean score of 0.674, 95% CI [0.183, 1.166], compared to the old age group ($p = .003$) for CF1 factor scores. In CF2 factor scores (Figure 4.13 B), the middle age group had a significantly higher mean score of 0.655, 95% CI [0.122, 1.188], compared to the old age group ($p = .010$). Moreover, the middle age group had a significantly higher mean CF4 score of 0.398, 95% CI [0.035, 0.760], compared to the young age group ($p = .026$) (Figure 4.13 D). There was no statistically significant age effect on the CF3 factor, and the effect size was small.

For sex differences, the analysis showed males have significantly higher scores than females in CF4 ($F(1,195) = 4.831$, $p = 0.029$, partial $\eta^2 = .024$, small effect) (Figure 4.12 D). No

significant effects of sex were found on the other three factor scores in the common fibular nerve, with trivial effect sizes (Figure 4.13 A, B&C).
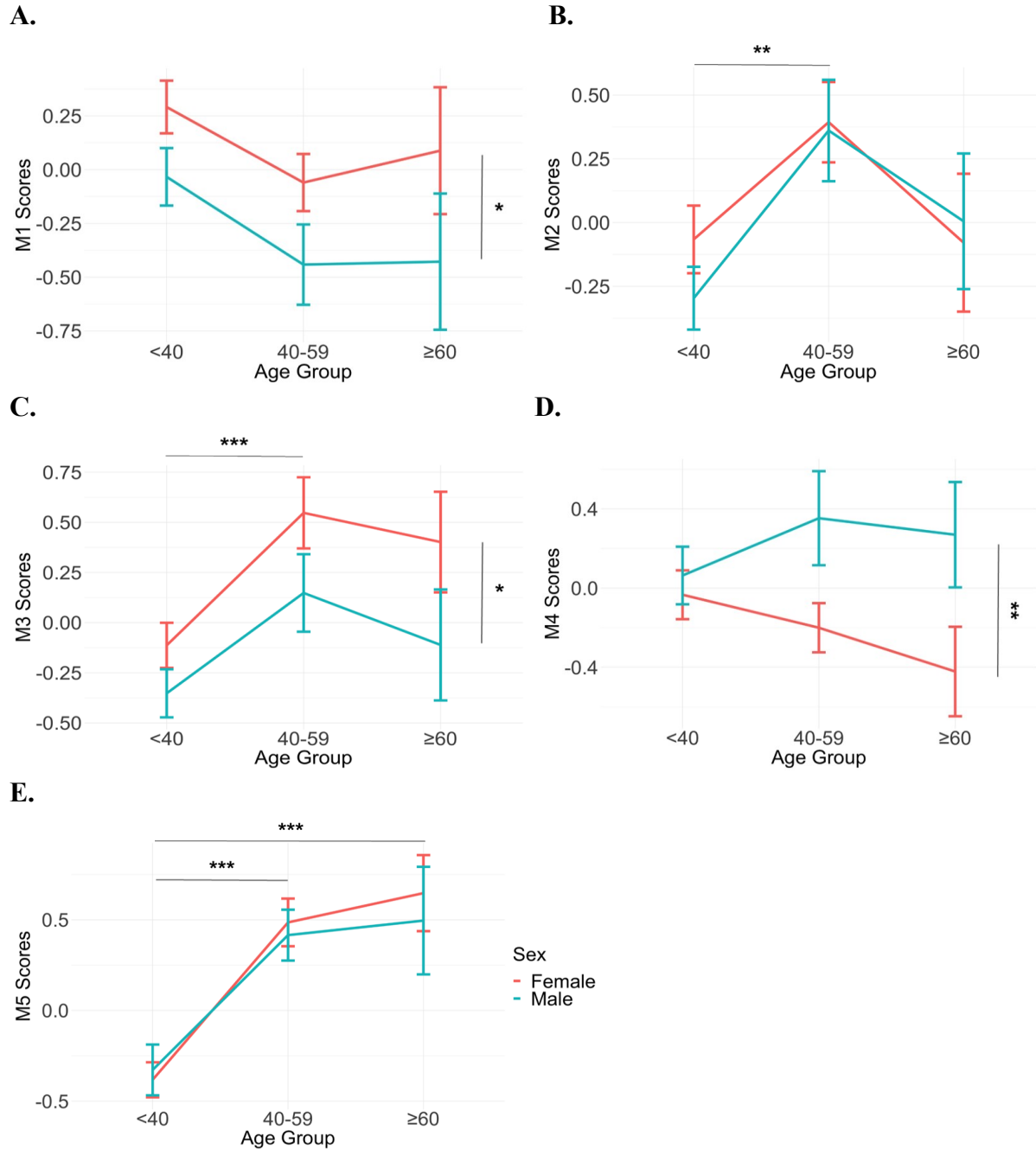
A.

B.

C.

D.
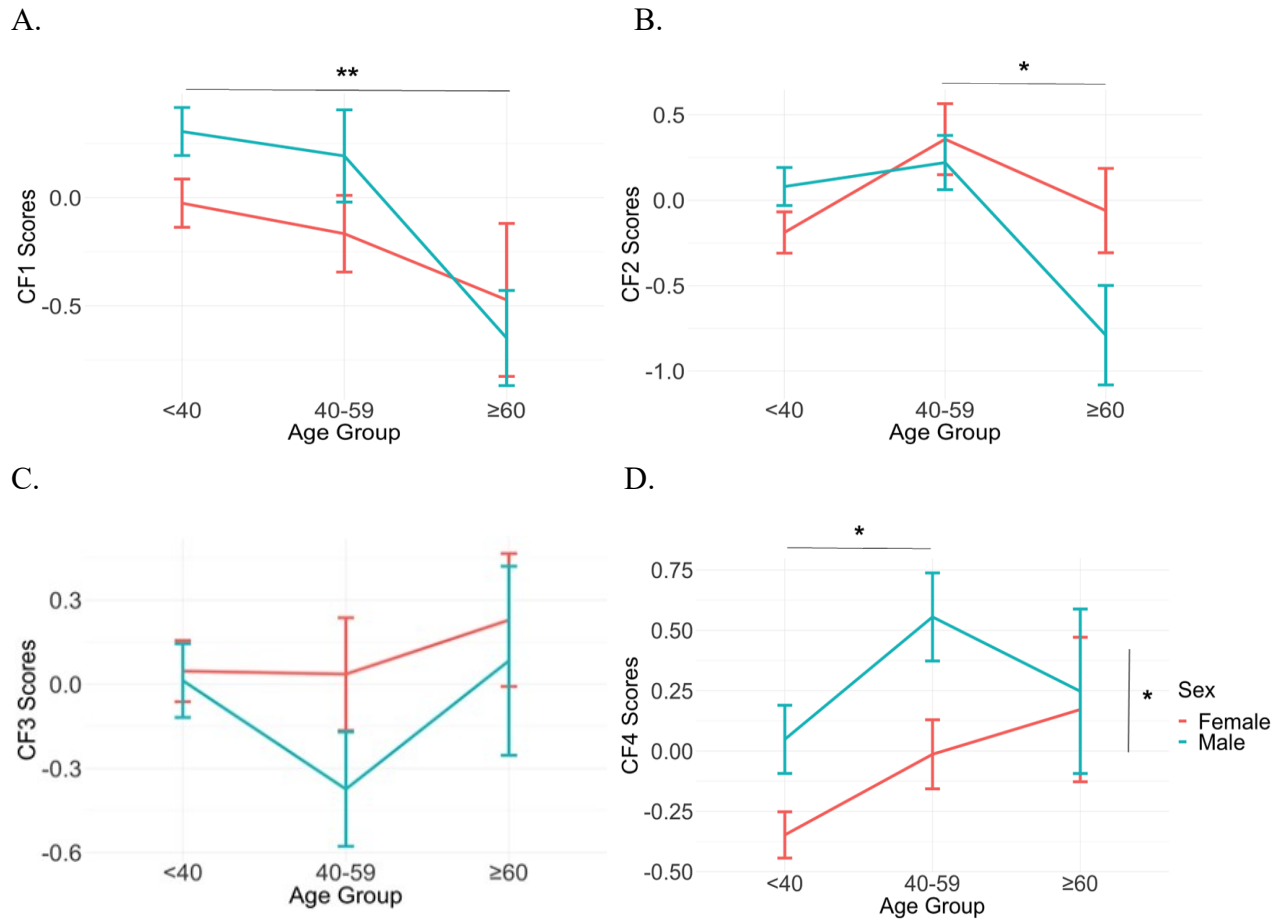
Figure 4.13 Line plots showing the effects of age and sex on the factor scores in the common fibular nerve. Age was categorized into three groups: <40 years (young), 40-59 years (middle-aged), and ≥60 years (old). A. CF1 factor scores in the common fibular nerve showed a significant age effect between the young and old groups. B. CF2 factor scores showed a significant age effect between the middle-aged and old groups. C. No effect of either age or sex on CF3. D. CF4 factor scores displayed significant effects of both age and sex. The age effect was significant between the young and middle-aged groups. Female factor scores are represented by the red line, while male factor scores are represented by the blue line. Significance level: * $p < 0.05$, ** $p < 0.01$, *** $p < 0.001$.

To summarize, in the common fibular nerve, the effects of age and sex on the factor scores are diverse and varied. But they are all small effects.

Comparing age and sex effects between the upper and lower limbs, age had a significant main effect in 4 out of 5 factors for the arm and 3 out of 4 factors for the leg. On the other hand,

sex showed a significant main effect in 3 out of 5 factors for the arm and 1 out of 4 factors for the leg. Specifically, age consistently influenced factors related to HCN channels (M2 & CF1) and nodal Ks channels (M3 & CF2) in both the upper and lower limbs. However, the relationship with age is quite different in the two limbs. In the arm, there was a positive correlation between the young and older age groups in the two factors, while in the leg, there was a negative correlation between the young or middle-aged and the older group. Additionally, sex had a significant effect on the Na^+ channels factor in both the arm (M4) and leg (CF4), with males showing higher values compared to females.

4.6 Diagnostic Utility of NET Factor Scores in ALS

To investigate the diagnostic utility of the factors derived from our analysis in clinical settings, we examined the factor scores for the ALS group and compared them with those of healthy controls in the middle-aged and old-age groups (older controls in Table 4.1).

To account for the influence of age and sex on the factor scores, we employed a one-way ANCOVA to explore the dissimilarities between healthy controls and people with ALS while accounting for these covariates. The ANCOVA was performed on each factor individually. For the median nerve, the results indicated a statistically significant difference between the two groups in the M1 score (F $(1, 91)$ = 6.733474, p = 0.011). Additionally, we calculated the effect size (unpaired Hedges' g) for group-only residuals between the controls and people with ALS, resulting in a value of 0.909 (large effect, Cohen, 1992) with a 95.0% CI of [0.189, 1.76] (Figure 4.14) (Ho et al., 2019). However, no statistically significant differences were observed in the other four factor scores in the median nerve between healthy controls and people with ALS (Hedge's g ranging from -0.454 to 0.19, small or trivial effects).
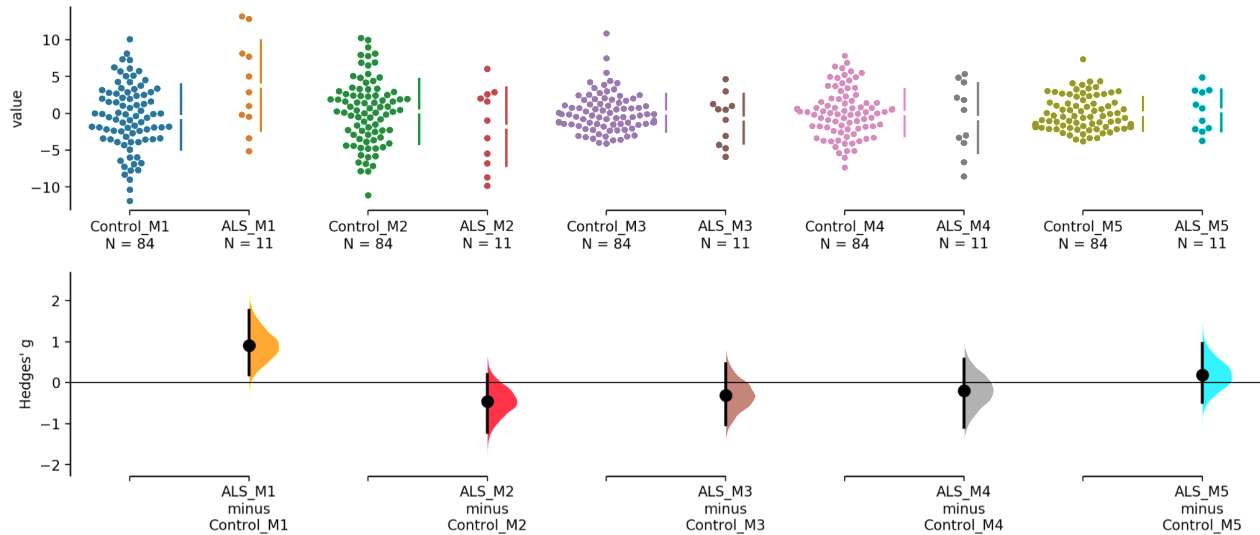
Figure 4.14 Comparison of factor scores in the median nerve between older healthy controls (≥ 40) and people diagnosed with ALS. The Hedges' g for 5 comparisons are shown in the above Cumming estimation plot. The raw data is plotted on the upper axes. The dots represent the group-only residuals of each individual. Each mean difference is plotted on the lower axes as a bootstrap sampling distribution. Mean differences are depicted as black dots; 95% confidence intervals are indicated by the ends of the vertical error bars. The error bar of the mean difference in the M1 scores does not hit zero (Hedges' g = 0.909, 95.0% CI [0.189, 1.76]. p=0.0052 for the two-sided permutation t-test), indicating a statistically significant and large difference between older controls and people with ALS, with ALS group having higher values on average.

In the common fibular nerve, to address the high missing rate in the refractoriness at 2ms in people diagnosed with ALS (Table 4.2, 7 out of 12 (58.3%) missing), we excluded this index from the normative data and conducted a new EFA. The factor structure remained similar after excluding this index. Subsequently, we recalculated the factor scores in the common fibular nerve without considering refractoriness at 2ms for both the control and ALS groups. Our analysis revealed no significant differences in common fibular nerve factor scores between the ALS group and the control group (Hedge's g ranging from -0.054 to 0.304, small or trivial effects) (Figure 4.15) (Ho et al., 2019).
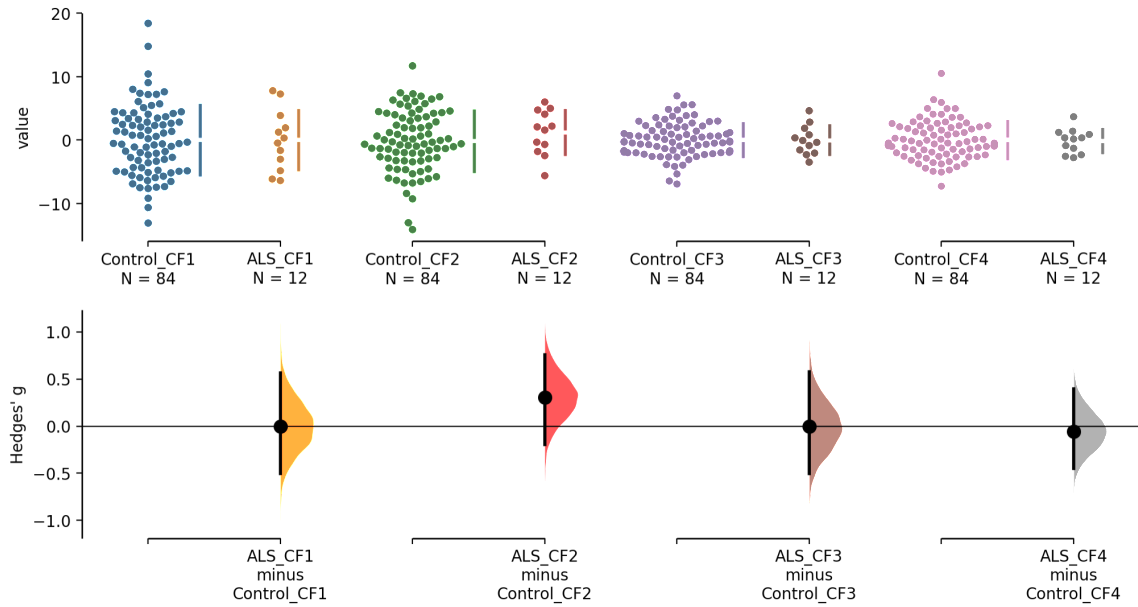
Figure 4.15 Comparison of factor scores in the common fibular nerve between older healthy controls (≥ 40) and people diagnosed with ALS. The Hedges' g for 4 comparisons are shown in the above Cumming estimation plot. The raw data is plotted on the upper axes. The dots represent the group-only residuals of each individual. Each mean difference is plotted on the lower axes as a bootstrap sampling distribution. Mean differences are depicted as black dots; 95% confidence intervals are indicated by the ends of the vertical error bars.

In summary, among all the factors analyzed, only the M1 factor (general potassium channels) in the median nerve demonstrated diagnostic utility in distinguishing between healthy controls and people diagnosed with ALS.

Chapter 5: Discussion

As a non-invasive technique to investigate nerve health, the *nerve excitability test* (NET) offers valuable insights into membrane properties and the activities of ion channels. Our study revealed that the 32 indices obtained from a NET in a single nerve are <u>interdependent</u> but the same indices are <u>independent</u> within an individual when comparing a nerve in the upper limb (median nerve) to the lower limb (common fibular nerve). The interdependence, or correlation, of the nerve indices, hinted at potential data redundancy and the possibility of underlying constructs that could be represented by a smaller number of factors. Exploratory Factor Analysis (EFA) found that >70% of the variance in the nerve excitability data could be summarized by five factors in the median nerve and four factors in the common fibular nerve. These factors changed with age and sex, and one of the factors in the median nerve was different between people living with a neurodegenerative condition (ALS) versus healthy controls. Altogether, the results of this thesis contribute to our understanding of nerve health by illuminating the relationships among nerve excitability indices and the diagnostic potential of NET through the process of dimension reduction.

5.1 Correlation Studies in Nerve Excitability Test

Over the more than twenty-three-year history since the introduction of the *nerve excitability test* (NET, also known as the TROND protocol, or colloquially as "*threshold-tracking*") (Bostock et al., 1998; Kiernan et al., 2000), basic and clinical researchers have used the test as an electrodiagnostic measure to provide insight into peripheral nerve pathophysiology. A significant milestone was the publication of consensus guidelines in 2020 (Kiernan et al., 2020) in the flagship journal of the International Federation of Clinical Neurophysiology, or IFCN. Currently, the software used to perform a NET (QTrac © UCL

Institute of Neurology, London, UK, available from Digitimer Ltd at www.Digitimer.com)

generates 32 nerve excitability indices from a complete test using the TROND protocol (see

Appendix, Table 2). Historically, neurophysiologists using the NET have informally

acknowledged that the 32 excitability indices are similar, yet statistical analysis in the

peer-reviewed literature has treated these indices as independent (Boerio et al., 2014;

Jankelowitz et al., 2007; Kuwabara et al., 2000), which increase the complexity of analysis and,

can be challenging for clinicians seeking meaningful insights. The work presented in this thesis

clearly shows that the 32 indices are strongly correlated within a nerve, but surprisingly not

between nerves in the same person.

The within-nerve correlations (Figures 4.2 & 4.3) could be subjectively grouped into two

categories: 1) expected, and 2) novel or surprising. Expected correlations included indices that

might be judged *redundant* by experts in the field. For example, in the Recovery Cycle

component of the NET, there are three indices that are reported for the phenomenon of

superexcitability: 1) Superexcitability (%, index #27 in Appendix Table 2), 2) Superexcitability

at 5 ms (%, index #31), and 3) Superexcitability at 7 ms (%, index #32). The average correlation

coefficient between these three indices was 0.94, which is classified as 'very strong'. This very

strong correlation is expected because these three indices all purport to measure the same nerve

excitability construct, superexcitability. In other words, these three indices are redundant. In the

present study, we addressed the redundancy by examining all the very strong correlations and

manually selecting one index from the pairs prior to conducting the EFA. This step was taken to

avoid multicollinearity, which could potentially compromise the reliability of the EFA model

(Kyriazos & Poga, 2023).

The second category of novel correlations provides new insights into the interrelationships of the 32 nerve excitability indices. For example, the undershoot part in the depolarizing threshold electrotonus is strongly negatively correlated with the overshoot part in the hyperpolarizing threshold electrotonus (r = -0.79 & -0.821 for median & common fibular nerve). One possible explanation for the negative correlation is the involvement of potassium (K^+) channels. At the end of the depolarizing conditioning pulse, the gradual deactivation of slow K^+ channels contributes to the undershoot phase of TEd. Some slow K^+ channels stayed open after the hyperpolarizing conditioning current stopped, involving in the overshoot phase of TEh by aiding the membrane potential return to its resting state (Nodera & Kaji, 2006).

We also observed more and stronger correlations within the common fibular than within the median nerve, particularly in the relationships between the indices in the subtests recovery cycle and threshold electrotonus. It might suggest an actual neurobiological difference between the upper and lower limb nerves, but the possibility of statistical artifacts cannot be completely ruled out. Conducting further analyses, considering the context of the nerve physiology (anatomical or functional differences), and assessing the stability of these correlations through various techniques (such as subgroup analysis, bootstrap resample or alternative statistical methods) can help determine whether this observation is indeed a statistical artifact or a meaningful pattern.

The correlations between nerves of the upper and lower limbs in the same person were also examined (Figure 4.4). The within-nerve correlations are conducive to the understanding of the between-nerve correlations. We are more interested in examining the correlations between the same indices in the two nerves. Although not very strong ($r < 0.6$), they to some degree

reveal intrinsic associations between the peripheral nerves from the upper and lower limbs in healthy individuals.

Our findings reveal that 24 out of the 32 on-diagonal correlations have a correlation coefficient (r) of 0.3 or higher (Table 4.4). Interestingly, when controlling for the covariate age through partial correlation analysis, the majority of these correlations diminished to smaller values, except for the minimum I/V slope ($r = 0.38$ to $r = 0.42$). This suggests that these between-nerve correlations may be influenced by their common association with age. Given that we controlled the temperature within the range of 32-34 ℃, the impact of temperature on these correlations is expected to be relatively minimal. The most possible biophysical factor influencing the minimum I/V slope is the presence of leak channels. As the minimum I/V slope is always positioned between the resting membrane potential (where some voltage-gated K+ channels and HCN channels are constitutively open alongside the leak channels), and the increasing hyperpolarizing phase (where the K^+ channels become deactivated and more HCN channels start to activate) (Benarroch, 2013; Kiernan et al., 2000). Additionally, the diameter of the axon is directly connected to the number of leak channels. Therefore, the retained correlation observed in the minimum I/V slope may imply that leak channels and the diameters of motor axons tend to be alike among individuals.

Our original hypothesis proposed a strong predictive connection between the NET indices in the upper and lower limbs, with a much lower expected variance within-subject compared to the between-subject. This strong correlation could potentially narrow the limits of anticipated values for a specific index in the leg when its value in the arm is known. This might improve the sensitivity to detect atypical results. Although the resemblance in covariance structures across the two nerves implies potential shared factors or common underlying

processes, the relatively weak correlations between the nerves restrict the potential of predicting values between limbs within individuals. This discrepancy indicates the distinct nature of nerve excitability properties between the upper and lower limb nerves. Thus, separate EFAs were performed for the median nerve and common fibular nerve.

5.2 Utility of Exploratory Factor Analysis in Nerve Excitability Test

While examining a correlation matrix can provide valuable information about the interconnections between NET indices, it is typically insufficient to discern whether an observed pattern of correlations corresponds to any meaningful structural representation of the data. With numerous correlations (496 correlation pairs for the 32 indices), identifying unexpected relationships may not be readily apparent by visualizing pairwise correlations. Factor analysis can tackle these challenges and improve understanding of the factors underpinning nerve excitability.

EFA successfully reduced the 16 selected indices in the NET dataset to 4 or 5 factors in the nerves from the upper and lower limbs. By identifying these latent factors, we are essentially identifying common constructs that explain the shared variance across multiple indices. This not only simplifies the data but also allows us to focus on the essential aspects of nerve excitability, making it easier to recognize the correlation patterns and draw meaningful conclusions from the findings. In essence, this streamlined approach through EFA provides a more concise and insightful representation of nerve function, enhancing our ability to understand and interpret the complex nature of nerve excitability in both upper and lower limb nerves.

EFA generated different models for the median and common fibular nerves (Figures 4.8 & 4.11). The 5-factor model for the median nerve and the 4-factor model for the common fibular nerve suggest that different latent constructs are responsible for upper and lower limb nerves. To

assign labels to the factors, we took into account the physiological basis (Appendix Table 1) and an axon model designed for interpreting nerve excitability studies (Jensen et al., 2008). A higher factor loading indicates a stronger relationship between the factor and the index. We primarily referred to the indices exhibiting higher loadings when labelling the factors, as they hold more substantial connections to the respective factors.

Within the median nerve, an additional factor M5 emerged named "passive electrical properties," which includes the strength duration time constant, TEh(10–20ms), and stimulus-response slope. However, it is important to note that this factor is relatively weak, as the loadings for each index are not very high (see Figure 4.8). Notably, TEh(10–20ms) showed a meaningful cross-loading of 0.38 (> 0.32, cf. MacCallum et al., 1999) to the M2 factor (HCN channels), and the communalities of stimulus-response slope and strength-duration time constant are less than 0.4 (0.14 and 0.37, respectively), indicating a weaker relationship with the other indices or the possibility of an additional factor that requires further exploration (Costello & Osborne, 2005). This emphasizes the need to interpret the M5 factor with caution.

In the common fibular nerve, the factor related to HCN channels includes more indices (such as 10–20ms in the hyperpolarizing threshold electrotonus and resting I/V slope) compared to the median nerve. This suggests a greater dominance of HCN channels in the excitability test during the earlier hyperpolarization and resting phase in the common fibular nerve. This is different from the finding that the lower limb demonstrated greater Ih conductance at a later phase of the hyperpolarizing currents (300ms) during hyperthermia as another hyperpolarizing stress (Marmoy et al., 2019). Additionally, the factor of superexcitability exhibits the highest loading on K^+ channels in the median nerve but on Na^+ channels in the common fibular nerve

according to the proposed factor labels in this study, suggesting there may be different ion channel contributions to the superexcitability in the two nerves.

Given NET indices represent the continuous interplay of various ion channels, the suitability of oblique rotation becomes evident, as it permits the presence of correlated factors and optimizes the comprehension of the factors' relationships. There are more correlations between factors in the median nerve than in the common fibular nerve. Specifically, in the common fibular nerve, only one correlation stands out, which is between CF1 (HCN channels) and CF4 (K^+ and Na_p channels). This correlation is negative ($r = -0.6$) because these channels open during the hyperpolarization and depolarization periods, respectively. This correlation is also present in the median nerve. For factors in the median nerve, there are moderate positive correlations observed between HCN channels and Na^+ channels, Na^+ channels and K^+ channels, as well as nodal K_s channels and the passive electrical properties, suggesting a closer interaction among the ion channels in the median nerve axons. These findings of the two factor models imply that the underlying mechanisms and ion channel activities in nerve excitability differ between the nerve in the upper limb and the nerve in the lower limb.

Another advantage factor analysis offered relevant to our study's context is closely tied to the concept of partitioning variance, which involves breaking down the variance present in measured variables into distinct components, including shared common variance, specific variance in individual variables, and random measurement error (Fabrigar & Wegener, 2011; Kline, 2013). It allowed us to partition out and understand the unique variances while focusing on the common variance attributed to the latent factors in NET indices. In this way, factor analysis aids in ensuring accurate and meaningful interpretation of factor scores. The derived factor scores for the healthy controls, coupled with the analysis of covariates, suggest that age

and sex impact certain factor scores in healthy controls, especially age effect on M5. These findings highlight the importance of considering age and sex as moderating variables in analyzing and interpreting factor scores.

Among all factors identified in the median and common fibular nerve, only one factor, M1 in the median nerve, exhibited a significant difference when comparing healthy controls to people diagnosed with ALS. M1 consists of five indices: TEd(40–60ms), TEd(90–100ms), TEd(10–20ms), superexcitability, and resting I/V slope. These indices fall within the seven proposed candidate biomarkers for LMN degeneration in ALS (Lugg et al., 2022). These biomarkers include prolonged SDTC, increased peak superexcitability, reduced peak subexcitability, greater threshold changes in response to depolarizing threshold electrotonus at 10–20ms, 40–60ms, and 90–100ms, greater threshold reduction during 50% depolarizing current, and reduced resting I/V slope. TEd(10–20ms), TEd(90–100ms), and superexcitability are among the four potential early biomarkers of ALS. Moreover, the observed alterations in the five indices within the M1 factor align with previous studies that have reported a decrease and dysfunction in K^+ channels among people diagnosed with ALS (Kanai et al., 2006). This indicates potential associations between these factors and the presence of the underlying condition.

5.3 Limitations

This study presents limitations from seven aspects, primarily on the characteristics of the samples and the methodology of data analysis. These limitations are going to be discussed in a sequential order.

1. **Healthy control sample considerations:** Regarding the sample size of healthy controls for the EFA, although both the median nerve and common fibular nerve models showed mean communalities above 0.7 (0.754 for the median nerve and 0.704 for the common fibular nerve),

there is one factor in the median nerve model has only two indices loading on it, suggesting that a larger sample size might be necessary to ensure reliability (Fabrigar & Wegener, 2011). The uneven distribution of healthy participants across age groups, with a larger proportion in the young group, could potentially affect the generalizability of the findings and limit the understanding of age-related effects on EFA factors.

2. **ALS sample considerations:** The relatively small sample size of the ALS group poses limitations. The post hoc analysis indicated a power of 0.6 for the medium effect size (Cohen's d = 0.72) in the difference between the ALS group and the similarly-aged control group (age ≥ 40 years) in the M1 factor, which suggests that the analysis is underpowered. To detect a medium effect size with a power of 0.8 and an α level of 0.05, a recommended sample size of 18 ALS and 134 controls would be necessary (Faul et al., 2007). The limited sample size may restrict the generalizability of the results to the broader ALS population. It may also lead to false-negative results for the other factors, meaning that we may not be able to detect existing differences. Furthermore, the ALS group mainly consists of slow progressors and they are not in the early stages of the disease. Additionally, the recordings were primarily taken from the better side of the body and often represented baseline data. This limitation restricts the ability to establish the sensitivity of identified factors for early ALS diagnosis.

3. **Peripheral nerves investigated**: This study focused on a specific subset of peripheral nerves, the median and common fibular nerves. The findings and conclusions drawn from this study can not be directly applicable to other peripheral nerves. Further investigation and study are required to expand our understanding of correlations and latent constructs underlying the nerve excitability in other peripheral nerves from both the upper and lower limbs.

4. **Data completeness and imputation**: The reliance on the complete dataset precludes the generation of factor scores when missing values are present, particularly for refractoriness at 2ms. This lack of flexibility limits a comprehensive analysis of the data and might lead to incomplete insights. Additionally, the imputation method employed in this study was originally tested for the normative median nerve and may not be optimized for the common fibular nerve or tailored to the ALS population. Consequently, there is a possibility of suboptimal imputation in the common fibular nerve dataset or potential missingness within the ALS dataset.

5. **Linear relationship assumptions:** EFA assumes that the observed variables are linearly related to the latent factors, which may not always hold true for the NET indices. In cases where the relationship between indices and factors is non-linear, EFA might not accurately capture the underlying structure of the data, leading to potential misinterpretation of the results.

6. **Labeling of the identified factors:** While the factor labels have been assigned based on the observed patterns of loadings and axon model work on NET results, they require further validation and testing. It is necessary to validate these labels by employing axon models to simulate ion channel conductance changes and their corresponding effects on the factors or through in-vitro experiments. This step would provide a more robust validation of the factors' underlying physiological mechanisms and ensure the accuracy of their labels.

7. **Preliminary Nature of EFA**: It's important to recognize that the EFA conducted represents an initial exploratory step rather than a conclusive solution. The fit indices of the models have not met the criteria for a good fit. This study serves as the essential first step in uncovering potential latent factors within the nerve excitability data. The model generating in factor analysis is an iterative process that involves refining and validating the identified factors. To ensure the

robustness and generalizability of the findings, it is necessary for future cross-validation and Confirmatory Factor Analysis (CFA) to further refine and validate the solution.

5.4 Conclusions

In conclusion, there are interdependencies among the nerve excitability testing (NET) indices within the median nerve and common fibular nerve. The presence of very strong correlations reflects redundancy that would burden the analysis and interpretation. Weak between-nerve correlations, or independency, underscore the distinct nature of nerve excitability in upper and lower limb nerves. Exploratory factor analysis (EFA) has the potential to identify the latent constructs and improve the interpretation of NET data. The number and nature of factors underlying NET indices in the upper and lower limbs are not the same. The factors can provide valuable insights into the underlying physiological constructs involved in nerve excitability. The recognition of a potential diagnostic factor in the median nerve provides valuable insights for both research and clinical applications.

References

Alberti, S., Gregorio, E. A., Spadella, C. T., & Cojocel, C. (2007). Localization and irregular distribution of Na,K-ATPase in myelin sheath from rat sciatic nerve. *TISSUE & CELL*, *39*(3), 195–201. https://doi.org/10.1016/j.tice.2007.03.004

Bae, J. S., Sawai, S., Misawa, S., Kanai, K., Isose, S., & Kuwabara, S. (2009). Differences in excitability properties of FDI and ADM motor axons. *Muscle & Nerve*, *39*(3), 350–354. https://doi.org/10.1002/mus.21107

Bae, J. S., Sawai, S., Misawa, S., Kanai, K., Isose, S., Shibuya, K., & Kuwabara, S. (2008). Effects of age on excitability properties in human motor axons. *Clinical Neurophysiology*, *119*(10), 2282–2286. https://doi.org/10.1016/j.clinph.2008.07.005

Baker, L. L., Wederich, Cynthia., McNeal, D. R., Newsam, C. J., & Waters, R. L. (2000). *Neuro muscular electrical stimulation: A practical guide* (4. ed.). Los Amigos Research & Education Institute; WorldCat.org.

Baker, M., Bostock, H., Grafe, P., & Martius, P. (1987). Function and distribution of three types of rectifying channel in rat spinal root myelinated axons. *The Journal of Physiology*, *383*(1), 45–67. https://doi.org/10.1113/jphysiol.1987.sp016395

Barrett, E., & Barrett, J. (1982). Intracellular recording from vertebrate myelinated axons: Mechanism of the depolarizing afterpotential. *JOURNAL OF PHYSIOLOGY-LONDON*, *323*(FEB), 117–144. https://doi.org/10.1113/jphysiol.1982.sp014064

Beckstein, O., Biggin, P., Bond, P., Bright, J., Domene, C., Grottesi, A., Holyoake, J., & Sansom, M. (2003). Ion channel gating: Insights via molecular simulations. *FEBS LETTERS*, *555*(1), 85–90. https://doi.org/10.1016/S0014-5793(03)01151-7

Bell, J. M. (2019). *Electrodiagnostic Nerve Tests: Understanding Healthy Peripheral Nerves*. 79.

Benarroch, E. E. (2013). HCN channels: Function and clinical implications. *Neurology*, *80*(3), 304–310.

Boerio, D., Bostock, H., Spescha, R., & Z'Graggen, W. J. (2014). Potassium and the Excitability Properties of Normal Human Motor Axons In Vivo. *PLOS ONE*, *9*(6). https://doi.org/10.1371/journal.pone.0098262

Bostock, H., & Bergmans, J. (1994). Post-tetanic excitability changes and ectopic discharges in a human motor axon. *Brain*, *117*(5), 913–928. https://doi.org/10.1093/brain/117.5.913

Bostock, H., Cikurel, K., & Burke, D. (1998). Threshold tracking techniques in the study of human peripheral nerve. *Muscle & Nerve*, *21*(2), 137–158.

Bostock, H., & Rothwell, J. (1997). Latent addition in motor and sensory fibres of human peripheral nerve. *JOURNAL OF PHYSIOLOGY-LONDON*, *498*(1), 277–294. https://doi.org/10.1113/jphysiol.1997.sp021857

Bostock, H., Sharief, M., Reid, G., & MURRAY, N. (1995). Axonal ion channel dysfunction in amyotrophic lateral sclerosis. *Brain*, *118*, 217–225. https://doi.org/10.1093/brain/118.1.217

Brink, E. E., & Mackel, R. G. (1993). Time course of action potentials recorded from single human afferents. *Brain*, *116*(2), 415–432. https://doi.org/10.1093/brain/116.2.415

Brooks, B. R. (1994). El Escorial World Federation of Neurology criteria for the diagnosis of amyotrophic lateral sclerosis. Subcommittee on Motor Neuron Diseases/Amyotrophic Lateral Sclerosis of the World Federation of Neurology Research Group on Neuromuscular Diseases and the El Escorial "Clinical limits of amyotrophic lateral sclerosis" workshop contributors. *Journal of the Neurological Sciences*, *124 Suppl*(jbj, 0375403), 96–107.

Brown, A. M., Schwindt, P. C., & Crill, W. E. (1994). Different voltage dependence of transient and persistent Na+ currents is compatible with modal-gating hypothesis for sodium channels. *Journal of Neurophysiology*, *71*(6), 2562–2565. https://doi.org/10.1152/jn.1994.71.6.2562

Browner, W. S., Newman, T. B., Cummings, S. R., & Grady, D. G. (2022). *Designing clinical research*. Lippincott Williams & Wilkins.

Burke, D., Howells, J., Trevillion, L., Kiernan, M. C., & Bostock, H. (2007). Inflections in threshold electrotonus to depolarizing currents in sensory axons. *MUSCLE & NERVE*, *36*(6), 849–852. https://doi.org/10.1002/mus.20862

Burke, D., Kiernan, M., & Bostock, H. (2001). Excitability of human axons. *CLINICAL NEUROPHYSIOLOGY*, *112*(9), 1575–1585. https://doi.org/10.1016/S1388-2457(01)00595-8

Caldwell, J., Schaller, K., Lasher, R., Peles, E., & Levinson, S. (2000). Sodium channel Na(v)1.6 is localized at nodes of Ranvier, dendrites, and synapses. *PROCEEDINGS OF THE NATIONAL ACADEMY OF SCIENCES OF THE UNITED STATES OF AMERICA*, *97*(10), 5616–5620. https://doi.org/10.1073/pnas.090034797

Casanova, I., Diaz, A., Pinto, S., & de Carvalho, M. (2014). Motor excitability measurements: The influence of gender, body mass index, age and temperature in healthy controls. *NEUROPHYSIOLOGIE CLINIQUE-CLINICAL NEUROPHYSIOLOGY*, *44*(2), 213–218. https://doi.org/10.1016/j.neucli.2014.03.002

Cattell, R. B. (1966). The scree test for the number of factors. *Multivariate Behavioral Research*, *1*(2), 245–276.

Cheah, B. C., Lin, C. S. Y., Park, S. B., Vucic, S., Krishnan, A. V., & Kiernan, M. C. (2012).

Progressive axonal dysfunction and clinical impairment in amyotrophic lateral sclerosis. *CLINICAL NEUROPHYSIOLOGY*, *123*(12), 2460–2467. https://doi.org/10.1016/j.clinph.2012.06.020

Child, D. (2006). *The essentials of factor analysis*. A&C Black.

Chiu, S. Y., & Ritchie, J. M. (1984). On the physiological role of internodal potassium channels and the security of conduction in myelinated nerve fibres. *Proceedings of the Royal Society of London. Series B. Biological Sciences*, *220*(1221), 415–422.

Cohen, J. (1969). *Statistical power analysis for the behavioral sciences*. Academic Press New York.

Cohen, J. (1992). A power primer. *Psychological Bulletin*, *112*(1), 155–159. https://doi.org/10.1037/0033-2909.112.1.155

Comrey, A. L., & Lee, H. B. (1992). *A first course in factor analysis, 2nd ed.* (pp. xii, 430). Lawrence Erlbaum Associates, Inc.

Costello, A. B., & Osborne, J. (2005). Best practices in exploratory factor analysis: Four recommendations for getting the most from your analysis. *Practical Assessment, Research, and Evaluation*, *10*, Article 7. https://doi.org/10.7275/JYJ1-4868

Crill, W. E. (1996). Persistent sodium current in mammalian central neurons. *Annual Review of Physiology*, *58*(1), 349–362.

DeCoster, J. (1998). *Overview of factor analysis*.

Devaux, J., Kleopa, K., Cooper, E., & Scherer, S. (2004). KCNQ2 is a nodal K+ channel. *Journal of Neuroscience*, *24*(5), 1236–1244. https://doi.org/10.1523/JNEUROSCI.4512-03.2004

DiStefano, C., Zhu, M., & Mîndrilă, D. (2009). Understanding and Using Factor Scores:

Considerations for the Applied Researcher. *Practical Assessment, Research &*
Evaluation., *14*, Article 20. https://doi.org/10.7275/DA8T-4G52

Dormann, C. F., Elith, J., Bacher, S., Buchmann, C., Carl, G., Carré, G., Marquéz, J. R. G.,
Gruber, B., Lafourcade, B., & Leitão, P. J. (2013). Collinearity: A review of methods to
deal with it and a simulation study evaluating their performance. *Ecography*, *36*(1),
27–46.

Everitt, B. S. (1975). Multivariate analysis: The need for data, and other problems. *The British*
Journal of Psychiatry, *126*(3), 237–240.

Fabrigar, L. R., & Wegener, D. T. (2011). *Exploratory Factor Analysis*. Oxford University Press.
https://doi.org/10.1093/acprof:osobl/9780199734177.001.0001

Fabrigar, L. R., Wegener, D. T., MacCallum, R. C., & Strahan, E. J. (1999). Evaluating the use of
exploratory factor analysis in psychological research. *Psychological Methods*, *4*(3), 272.

Faul, F., Erdfelder, E., Lang, A.-G., & Buchner, A. (2007). G*Power 3: A flexible statistical
power analysis program for the social, behavioral, and biomedical sciences. *Behavior*
Research Methods, *39*(2), 175–191. https://doi.org/10.3758/BF03193146

Feldman, E. L., Stevens, M. J., Thomas, P. K., Brown, M. B., Canal, N., & Greene, D. A. (1994).
A Practical Two-Step Quantitative Clinical and Electrophysiological Assessment for the
Diagnosis and Staging of Diabetic Neuropathy. *Diabetes Care*, *17*(11), 1281–1289.
https://doi.org/10.2337/diacare.17.11.1281

Field, A. P. (2009). *Discovering statistics using SPSS: And sex, drugs and rock "n" roll* (3rd ed).
SAGE Publications.

Geevasinga, N., Menon, P., Howells, J., Nicholson, G. A., Kiernan, M. C., & Vucic, S. (2015).
Axonal Ion Channel Dysfunction in C9orf72 Familial Amyotrophic Lateral Sclerosis.

JAMA NEUROLOGY, *72*(1), 49–57. https://doi.org/10.1001/jamaneurol.2014.2940

Glenn, T. D., & Talbot, W. S. (2013). Signals regulating myelination in peripheral nerves and the

    Schwann cell response to injury. *Current Opinion in Neurobiology*, *23*(6), 1041–1048.

    https://doi.org/10.1016/j.conb.2013.06.010

Gorsuch, R. L. (1983). *Factor analysis.* (2nd Edition). Psychology Press.

    https://doi.org/10.4324/9780203781098

Hedges, L. V. (1981). Distribution Theory for Glass's Estimator of Effect size and Related

    Estimators. *Journal of Educational Statistics*, *6*(2), 107–128.

    https://doi.org/10.3102/10769986006002107

Henson, R. K., & Roberts, J. K. (2006). Use of Exploratory Factor Analysis in Published

    Research: Common Errors and Some Comment on Improved Practice. *Educational and*

    Psychological Measurement, *66*(3), 393–416. https://doi.org/10.1177/0013164405282485

Ho, J., Tumkaya, T., Aryal, S., Choi, H., & Claridge-Chang, A. (2019). Moving beyond P values:

    Data analysis with estimation graphics. *Nature Methods*, *16*(7), 565–566.

    https://doi.org/10.1038/s41592-019-0470-3

Horn, J. L. (1965). A rationale and test for the number of factors in factor analysis.

    Psychometrika, *30*, 179–185.

Howells, J., Matamala, J. M., Park, S. B., Garg, N., Vucic, S., Bostock, H., Burke, D., &

    Kiernan, M. C. (2018). In vivo evidence for reduced ion channel expression in motor

    axons of patients with amyotrophic lateral sclerosis. *The Journal of Physiology*, *596*(22),

    5379–5396.

Hu, L., & Bentler, P. M. (1999). Cutoff criteria for fit indexes in covariance structure analysis:

    Conventional criteria versus new alternatives. *Structural Equation Modeling: A*

Multidisciplinary Journal, *6*(1), 1–55.

IBM Corp. (2015). *IBM SPSS Statistics for Windows, Version 23.0*. IBM Corp.

Jankelowitz, S. K., & Burke, D. (2009). Axonal excitability in the forearm: Normal data and

differences along the median nerve. *Clinical Neurophysiology*, *120*(1), 167–173.

https://doi.org/10.1016/j.clinph.2008.08.017

Jankelowitz, S. K., McNulty, P. A., & Burke, D. (2007). Changes in measures of motor axon

excitability with age. *Clinical Neurophysiology*, *118*(6), 1397–1404.

https://doi.org/10.1016/j.clinph.2007.02.025

Jensen, K., Luu, T. N., & Jones, K. E. (2008). Using axon models to interpret electrodiagnostic

nerve tests. *BMC Neuroscience*, *9*, P43. https://doi.org/10.1186/1471-2202-9-S1-P43

Jolliffe, I. T. (2005). Factor Analysis, Overview. In P. Armitage & T. Colton (Eds.), *Encyclopedia

of Biostatistics* (1st ed.). Wiley. https://doi.org/10.1002/0470011815.b2a13024

Kaiser, H. F. (1960). The application of electronic computers to factor analysis. *Educational and

Psychological Measurement*, *20*(1), 141–151.

Kaiser, H. F. (1974). An index of factorial simplicity. *Psychometrika*, *39*(1), 31–36.

https://doi.org/10.1007/BF02291575

Kanai, K., Kuwabara, S., Misawa, S., Tamura, N., Ogawara, K., Nakata, M., Sawai, S., Hattori,

T., & Bostock, H. (2006). Altered axonal excitability properties in amyotrophic lateral

sclerosis: Impaired potassium channel function related to disease stage. *Brain*, *129*(4),

953–962.

Kang, H. (2013). The prevention and handling of the missing data. *Korean Journal of

Anesthesiology*, *64*(5), 402. https://doi.org/10.4097/kjae.2013.64.5.402

Kiernan, M., Burke, D., Andersen, K., & Bostock, H. (2000). Multiple measures of axonal

excitability: A new approach in clinical testing. *MUSCLE & NERVE*, *23*(3), 399–409.

https://doi.org/10.1002/(SICI)1097-4598(200003)23:3<399::AID-MUS12>3.0.CO;2-G

Kiernan, M. C., Bostock, H., Park, S. B., Kaji, R., Krarup, C., Krishnan, A. V., Kuwabara, S.,

Lin, C. S.-Y., Misawa, S., Moldovan, M., Sung, J., Vucic, S., Wainger, B. J., Waxman, S.,

& Burke, D. (2020). Measurement of axonal excitability: Consensus guidelines. *Clinical*

Neurophysiology, *131*(1), 308–323. https://doi.org/10.1016/j.clinph.2019.07.023

Kiernan, M. C., & Lin, C. S. Y. (2012). Nerve Excitability. In *Aminoff's Electrodiagnosis in*

Clinical Neurology (pp. 345–365). Elsevier.

https://doi.org/10.1016/B978-1-4557-0308-1.00015-7

Kiernan, M., Cikurel, K., & Bostock, H. (2001). Effects of temperature on the excitability

properties of human motor axons. *BRAIN*, *124*, 816–825.

https://doi.org/10.1093/brain/124.4.816

Kiernan, M., Mogyoros, I., Hales, J., Gracies, J., & Burke, D. (1997). Excitability changes in

human cutaneous afferents induced by prolonged repetitive axonal activity. *JOURNAL*

OF PHYSIOLOGY-LONDON, *500*(1), 255–264.

https://doi.org/10.1113/jphysiol.1997.sp022015

Kim, S. (2015). *ppcor: Partial and Semi-Partial (Part) Correlation* (R package version 1.1).

https://CRAN.R-project.org/package=ppcor

Klein, C. S., Zhao, C. N., Liu, H., & Zhou, P. (2018). Differences in excitability properties

between medial gastrocnemius, tibialis anterior, and abductor pollicis brevis motor axons.

Muscle & Nerve, *57*(1). https://doi.org/10.1002/mus.25722

Kline, R. (2013). Exploratory and confirmatory factor analysis. *Applied Quantitative Analysis in*

the Social Sciences, 171–207.

Kovalchuk, M. O., Franssen, H., Van Schelven, L. J., & Sleutjes, B. T. H. M. (2018). Comparing

    excitability at 37°C versus at 20°C: Differences between motor and sensory axons.

    Muscle & Nerve, *57*(4), 574–580. https://doi.org/10.1002/mus.25960

Kubo, Y., Adelman, J., Clapham, D., Jan, L., Karschin, A., Kurachi, Y., Lazdunski, M., Nichols,

    C., Seino, S., & Vandenberg, C. (2005). International Union of Pharmacology. LIV.

    Nomenclature and molecular relationships of inwardly rectifying potassium channels.

    PHARMACOLOGICAL REVIEWS, *57*(4), 509–526. https://doi.org/10.1124/pr.57.4.11

Kuwabara, S. (2001). Differences in accommodative properties of median and peroneal motor

    axons. *Journal of Neurology, Neurosurgery & Psychiatry*, *70*(3), 372–376.

    https://doi.org/10.1136/jnnp.70.3.372

Kuwabara, S., Cappelen-Smith, C., Lin, C. S.-Y., Mogyoros, I., Bostock, H., & Burke, D. (2000).

    Excitability properties of median and peroneal motor axons. *Muscle & Nerve*, *23*(9),

    1365–1373.

    https://doi.org/10.1002/1097-4598(200009)23:9<1365::AID-MUS7>3.0.CO;2-1

Kuwabara, S., Misawa, S., Kanai, K., Tamura, N., Nakata, M., Sawai, S., & Hattori, T. (2007).

    The effects of physiological fluctuation of serum potassium levels on excitability

    properties in healthy human motor axons. *Clinical Neurophysiology*, *118*(2), 278–282.

    https://doi.org/10.1016/j.clinph.2006.10.009

Kyriazos, T., & Poga, M. (2023). Dealing with Multicollinearity in Factor Analysis: The

    Problem, Detections, and Solutions. *Open Journal of Statistics*, *13*(3), 404–424.

Lin, C., Kuwabara, S., Cappelen-Smith, C., & Burke, D. (2002). Responses of human sensory

    and motor axons to the release of ischaemia and to hyperpolarizing currents. *JOURNAL*

    OF PHYSIOLOGY-LONDON, *541*(3), 1025–1039.

https://doi.org/10.1113/jphysiol.2002.017848

Little, R. J. A., & Rubin, D. B. (2002). Statistical Analysis with Missing Data. *John Wiley & Sons.*, *793*, 7.

Lüdecke, D. (2023). *sjPlot: Data Visualization for Statistics in Social Science* (R package version 2.8.14). https://CRAN.R-project.org/package=sjPlot

Lugg, A., Schindle, M., Sivak, A., Tankisi, H., & Jones, K. E. (2022). *Nerve excitability as a biomarker for amyotrophic lateral sclerosis: A systematic review and meta-analysis* [Preprint]. Neurology. https://doi.org/10.1101/2022.02.11.22270866

Luu, M. J., Jones, K. E., & Collins, D. F. (2021). Decreased excitability of motor axons contributes substantially to contraction fatigability during neuromuscular electrical stimulation. *Applied Physiology, Nutrition, and Metabolism*, *46*(4), 346–355. https://doi.org/10.1139/apnm-2020-0366

MacCallum, R. C., Widaman, K. F., Preacher, K. J., & Hong, S. (2001). Sample size in factor analysis: The role of model error. *Multivariate Behavioral Research*, *36*(4), 611–637.

MacCallum, R. C., Widaman, K. F., Zhang, S., & Hong, S. (1999). Sample size in factor analysis. *Psychological Methods*, *4*(1), 84.

Marmoy, O. R., Furlong, P. L., & Moore, C. E. G. (2019). Upper and lower limb motor axons demonstrate differential excitability and accommodation to strong hyperpolarizing currents during induced hyperthermia. *Journal of Neurophysiology*, *121*(6), 2061–2070. https://doi.org/10.1152/jn.00464.2018

McHugh, J. C., Reilly, R. B., & Connolly, S. (2011). Examining the effects of age, sex, and body mass index on normative median motor nerve excitability measurements. *Clinical Neurophysiology*, *122*(10), 2081–2088. https://doi.org/10.1016/j.clinph.2011.03.020

Medical Research Council. (1943). *Aids to the examination of the peripheral nervous system*. HMSO, London.

Mogyoros, I. (1997). Excitability changes in human sensory and motor axons during hyperventilation and ischaemia. *Brain*, *120*(2), 317–325. https://doi.org/10.1093/brain/120.2.317

Moosmang, S., Stieber, J., Zong, X., Biel, M., Hofmann, F., & Ludwig, A. (2001). Cellular expression and functional characterization of four hyperpolarization-activated pacemaker channels in cardiac and neuronal tissues: HCN channel expression and characterization. *European Journal of Biochemistry*, *268*(6), 1646–1652. https://doi.org/10.1046/j.1432-1327.2001.02036.x

Nodera, H., & Kaji, R. (2006). Nerve excitability testing and its clinical application to neuromuscular diseases. *Clinical Neurophysiology : Official Journal of the International Federation of Clinical Neurophysiology*, *117*(9), 1902–1916.

Nunnally, J. D. (1978). *Psychometric Theory (2nd ed), New York: McGraw-Hill.* https://api.semanticscholar.org/CorpusID:166821603

R Core Team. (2023). *R: A language and environment for statistical computing.* R Foundation for Statistical Computing. https://www.R-project.org/

Revelle, W. (2023). *psych: Procedures for Psychological, Psychometric, and Personality Research* (R package version 2.3.3). Northwestern University. https://CRAN.R-project.org/package=psych

Ritchie, J. M., & Chiu, S. Y. (1981). Distribution of sodium and potassium channels in mammalian myelinated nerve. *Advances in Neurology*, *31*(2nx, 0367524), 329–342.

Robinson, L. R., Rubner, D. E., Wahl, P. W., Fujimoto, W. Y., & Stolov, W. C. (1992). FACTOR

ANALYSIS: Methodology for Data Reduction in Nerve Conduction Studies. *American Journal of Physical Medicine & Rehabilitation*, *71*(1), 22–27.

Rowland, L. P., & Shneider, N. A. (2001). Amyotrophic lateral sclerosis. *The New England Journal of Medicine*, *344*(22), 1688–1700.

Schober, P., Boer, C., & Schwarte, L. A. (2018). Correlation Coefficients: Appropriate Use and Interpretation. *Anesthesia & Analgesia*, *126*(5). https://journals.lww.com/anesthesia-analgesia/Fulltext/2018/05000/Correlation_Coefficients__Appropriate_Use_and.50.aspx

Schwarz, J. R., Glassmeier, G., Cooper, E. C., Kao, T.-C., Nodera, H., Tabuena, D., Kaji, R., & Bostock, H. (2006). KCNQ channels mediate IKs, a slow K+ current regulating excitability in the rat node of Ranvier. *The Journal of Physiology*, *573*(1), 17–34.

Schwarz, J. R., Reid, G., & Bostock, H. (1995). Action potentials and membrane currents in the human node of Ranvier. *Pflügers Archiv European Journal of Physiology*, *430*(2), 283–292. https://doi.org/10.1007/BF00374660

Skou, J. C. (1957). The influence of some cations on an adenosine triphosphatase from peripheral nerves. *Biochimica et Biophysica Acta*, *23*, 394–401.

Skou, J. C. (1965). Enzymatic basis for active transport of Na+ and K+ across cell membrane. *Physiological Reviews*, *45*(3), 596–618.

Spearman, C. (1904). "General Intelligence," Objectively Determined and Measured. *American Journal of Psychol Ogy 5*, 201–293.

Spillane, J., Kullmann, D. M., & Hanna, M. G. (2016). Genetic neurological channelopathies: Molecular genetics and clinical phenotypes. *Journal of Neurology, Neurosurgery & Psychiatry*, *87*(1), 37. https://doi.org/10.1136/jnnp-2015-311233

Stevens, J. (1992). *Applied multivariate statistics for the social sciences, 2nd ed.* (pp. xvii, 629).

Lawrence Erlbaum Associates, Inc.

Tabachnick, B. G., & Fidell, L. S. (2007). *Using multivariate statistics, 5th ed.* (pp. xxvii, 980).

Allyn & Bacon/Pearson Education.

The MathWorks Inc. (2022). *MATLAB version: 9.13.0 (R2022b)*. The MathWorks Inc.

https://www.mathworks.com

Thurstone, L. L. (1934). The vectors of mind. *Psychological Review*, *41*(1), 1.

Thurstone, L. L. (1947). *Multiple-Factor Analysis-A Development and Expansion of the Vectors*

of Mind, The University of Chicago Press, Chicago Illinois.

Wang, H., Kunkel, D. D., Martin, T. M., Schwartzkroin, P. A., & Tempel, B. L. (1993).

Heteromultimeric K+ channels in terminal and juxtaparanodal regions of neurons.

Nature, *365*(6441), 75–79.

Wei, T., & Simko, V. (2021). *R package "corrplot": Visualization of a Correlation Matrix*

(Version 0.92). https://github.com/taiyun/corrplot

West, S. G., Finch, J. F., & Curran, P. J. (1995). Structural equation models with nonnormal

variables: Problems and remedies. In *Structural equation modeling: Concepts, issues,*

and applications. (pp. 56–75). Sage Publications, Inc.

Yong, A. G., & Pearce, S. (2013). A Beginner's Guide to Factor Analysis: Focusing on

Exploratory Factor Analysis. *Tutorials in Quantitative Methods for Psychology*, *9*(2),

79–94. https://doi.org/10.20982/tqmp.09.2.p079

Appendix

Table 1 Physiological basis of the nerve excitability indices, differences in the upper limb compared to the lower limb, and changes due to influencing factors.

Properties	Physiology basis	Age↑[a]	Sex (Female compared to Male)[a]	Temperature↓[a]	Serum K⁺ ↑[a]	Upper limb compared to lower limb[b]
1 Peak response	CMAPmax	↓(McHugh 2011; Casanova 2014)				↑(Klein 2018)
2 Stimulus for 50% max response	Transient Na⁺ channels	↑(Jankelowitz 2007)				↓(Kuwabara 2000; Klein 2018)
3 Stimulus-response\slope	Threshold discrepancy between axons	↓(Jankelowitz 2007; McHugh 2011; Casanova 2014)				↑(Klein 2018)
4 Latency	Conduction velocity and distance			↑(Kiernan 2001)		
5 Rheobase	Persistent and transient Na⁺ channels	↑(Jankelowitz 2007)	↓(Bae 2008)			↓(Klein 2018)
6 Strength-duration\time constant	Persistent Na⁺ channels (positive related) open at RMP; the rate at which threshold current increases as the duration of the test stimulus is reduced to zero	↑(Bae 2008)		↑(Kovakchuk 2017; Kiernan 2001)		
7 TEd(10–20ms)	Activation of persistent Na⁺ channels Limit by the open of fast K⁺ channels (Kv1)				↓(Boërio 2014)	↑(Klein 2018)
8 TEh(10–20ms)	Closure of channels active at rest (mainly the persistent Na⁺ current and the slow K⁺ current)				↑(Boërio 2014)	↑(Klein 2018)
9 TEd20(10–20ms)	Same as 07				↓(Boërio 2014)	

10 TEh20(10–20ms)	Same as 08				↑(Boërio 2014)	
11 TEd(peak)	Open of slow K^+ channels (Kv7)	↑(Bae 2008)		↓(Kovakchuk 2017)	↓(Boërio 2014)	↑(Kuwabara 2000; Kuwabara 2001; Klein 2018)
12 TEh(20–40ms)	I_h current					
13 TEd20(peak)	Same as 11				↓(Boërio 2014)	
14 TEd(40–60ms)	Accomodative effect of slow K^+ channels			↑(Kiernan 2001)		
15 TEd(90–100ms)	Balance between depolarizing current and the opening of slow K^+ channels trying to hyperpolarize	↓(Bae 2008; McHugh 2011)			↓(Kuwabara 2007)	↑(Klein 2018)
16 TEh(90–100ms)	Open of HCN channels			↓(Kovakchuk 2017)	↑(Boërio 2014)	↓(Klein 2018)
17 TEd40(Accom)	Slow K^+					↑(Kuwabara 2000)
18 Accommodation half-time	Slow K^+ properties	↓(Casanova 2014)	↓(McHugh 2011)	↑(Kovakchuk 2017; Kiernan 2001)		
19 S2 accommodation	Slow K^+			↓(Kovakchuk 2017)		↑(Klein 2018; Kuwabara 2000)
20 TEh(slope 101-140ms)	Gradual closure of HCN channels and re-activation of persistent Na^+ channels					
21 TEd(undershoot)	Slow deactivation of slow K^+ channels		↑(McHugh 2011)	↓(Kiernan 2001)		↑(Kuwabara 2000)
22 TEh(overshoot)	Slow deactivation of Ih and the reactivation of slow K^+ channels			↓(Kiernan 2001)	↑(Kuwabara 2007)	↑(Kuwabara 2000)

23 Resting I/V slope	resting input conductance (affected by channels open at resting membrane potential)	↑(Bae 2008)		↑(Kovakchuk 2017)	↑(Boërio 2014)	
24 Minimum I/V slope	Leak channels	↑(Jankelowitz 2007; Bae 2008; McHugh 2011)	↑Bae 2008	↑(Kovakchuk 2017)		↓(Klein 2018)
25 Hyperpolarizing I/V slope	Ih current by HCN channels	↑(Jankelowitz 2007; Bae 2008; McHugh 2011)	↑Bae 2008			
26 RRP	recovery of transient Na$^+$ channels			↑(Kiernan 2001)	↑(Kuwabara 2007; Boërio 2014)	↓(Klein 2018)
27 Superexcitability	depolarizing afterpotential (Activity of fast K$^+$ channels)	↓(Jankelowitz 2007; Bae 2008; McHugh 2011)	↑(Bae 2008; McHugh 2011)		↓(Kuwabara 2007; Boërio 2014)	↑(Klein 2018)
28 Subexcitability	closure of slow K$^+$ channels (mix with decaying superexcitability)		↑(Bae 2008; McHugh 2011)			↑(Kuwabara 2000; Klein 2018)
29 Refractoriness at 2 ms	Recovery rate of Na$^+$ channels					
30 Refractoriness at 2.5ms	Recovery rate of Na$^+$ channels	↓(Jankelowitz 2007)				
31 Superexcitability at 5 ms	Different point to look at the shift					
32 Superexcitability at 7 ms						↑(Kuwabara 2000)

↓: lower/decrease. ↑: higher/increase. [a]Measurements were made at the median nerve. [b]Measurements were made at the median nerve at the wrist vs the peroneal nerve at the knee. CMAPmax: maximum of the compound muscle action potential. RRP: relative refractory period.

Table 2 Nerve Excitability Test graphs and indices of one participant's median nerve retrieved from QTracP. Graphs are shown: A. stimulus-response curve, B. strength-duration relationship C. threshold electrotonus, D. current-threshold relationship (threshold I/V), and E. recovery cycle

A. Stimulus-Response	B. Strength-Duration	C. Threshold Electrotonus	D. Threshold I/V	E. Recovery Cycle

1 Peak response (mv)	5 Rheobase (mA)	7 TEd(10–20ms)	23 Resting I/V slope	26 Relative refractory period (RRP)
2 Stimulus (mA) for 50% max	6 Strength-duration\time constant	8 TEh(10–20ms)	24 Minimum I/V slope	(ms)
response	(ms)	9 TEd20(10–20ms)	25 Hyperpol. I/V slope	27 Superexcitability (%)
3 Stimulus-response\slope		10 TEh20(10–20ms)		28 Subexcitability (%)
4 Latency (ms) (not shown)		11 TEd(peak)		29 Refractoriness at 2 ms (%)
		12 TEh(20–40ms)		30 Refractoriness at 2.5ms (%)
		13 TEd20(peak)		31 Superexcitability at 5 ms (%)
		14 TEd(40–60ms)		32 Superexcitability at 7 ms (%)
		15 TEd(90–100ms)		
		16 TEh(90–100ms)		
		17 TEd40(Accom)		
		18 Accommodation half-time (ms)		
		19 S2 accommodation		
		20 TEh(slope 101-140ms)		
		21 TEd(undershoot)		
		22 TEh(overshoot)		

Table 3 Demographic and clinical characteristics of people diagnosed with ALS.

Patient	Sex	Age (y)	Onset	Date symptom onset	Date of diagnosis	Date of Baseline NET	Family history	FVC%	ALSFRS-R at Baseline
1	M	67	U	1/1/2018	11/22/2018	6/22/2021	N	83	45
2	F	60	L	7/1/2020	6/10/2021	10/19/2021	N	93	46
3	M	54	U	6/1/2020	12/1/2020	11/12/2021	N	105	42
4	M	53	L	6/1/2018	10/30/2018	1/26/2022	Y	98	48
5	M	55	L	6/1/2017	10/31/2017	2/8/2022	N	70	42
6	F	70	UL	1/1/2013	9/1/2014	3/9/2022	Y	78	38
7	M	75	U	7/1/2020	5/4/2021	3/23/2022	N	64	39
8	M	70	L	7/1/1995	10/1/2018	4/13/2022	N	86	43
9	F	53	U	10/1/2021	4/1/2022	9/6/2022	N	102	42
10	F	67	U	10/1/2020	4/1/2021	9/15/2022	N	70	35
11	F	62	B	5/1/2021	4/1/2022	9/21/2022	N	116	44
12	M	63	L	1/1/2019	2/1/2020	9/27/2022	N	83	38
13	M	47	L	5/1/2021	9/13/2022	11/22/2022	N	111	47
14	F	64	L	7/1/2015	10/1/2020	1/25/2023	Y	101	42
15	M	68	U	10/1/2021	12/1/2022	2/10/2023	Y	71	35
Average	M (60%)	61.87						88.73	41.73

Table 4 Standardized factor loadings for each index after oblique rotation in the median nerve.

Index	M1	M2	M3	M4	M5
TEd(40–60ms)	**0.9592**	0.0137	-0.1773	0.3838	-0.2407
TEd(90–100ms)	**0.9310**	0.0426	-0.4059	-0.0010	0.2157
Superexcitability	**-0.6770**	-0.0368	-0.4120	0.2521	0.5675
TEd(10–20ms)	**0.6083**	-0.1246	0.2265	-0.1026	0.1565
Resting I/V slope	**-0.5069**	0.4388	0.2815	0.0925	-0.0867
TEh(90–100ms)	-0.1504	**0.8943**	0.0082	0.0320	0.0234
Minimum I/V slope	0.1398	**0.8863**	0.0194	-0.2043	0.2871
TEh(slope 101-140ms)	0.0228	**-0.6604**	0.2189	-0.1391	0.2810
TEd(undershoot)	0.0801	0.2287	**-0.9417**	-0.1814	0.0846
TEh(overshoot)	0.0049	0.0956	**0.8414**	0.2500	0.1103
Subexcitability	-0.2508	0.0973	**0.5472**	-0.0927	0.1257
RRP	-0.0638	-0.0750	0.0491	**1.0238**	0.2596
Refractoriness at 2 ms	0.2115	-0.0117	0.3111	**0.9705**	0.0944
SDTC	0.1987	0.1412	0.1376	0.1372	**0.5448**
TEh(10–20ms)	-0.2364	0.3849	-0.1637	0.2216	**-0.4532**
Stimulus-response\slope	0.1493	0.0217	0.0134	-0.0538	**-0.3602**

The highest factor loading for each index were bolded. RRP: relative refractory period. SDTC: Strength-duration time constant.

Table 5 Standardized factor loadings for each index after oblique rotation in the common fibular nerve.

Index	CF1	CF2	CF3	CF4
TEh(slope 101-140ms)	**-0.9915**	0.3604	-0.2168	-0.0273
TEh(10–20ms)	**0.9335**	-0.2015	0.0550	0.0273
TEh(90–100ms)	**0.8414**	0.0332	-0.0861	0.0826
Resting I/V slope	**0.5172**	0.1597	-0.3826	0.0800
Minimum I/V slope	**0.4941**	0.0838	-0.0254	-0.2109
TEd(undershoot)	0.1321	**-0.8996**	0.2043	0.2603
TEh(overshoot)	-0.0434	**0.8964**	-0.3229	-0.0983
SDTC	-0.0152	**0.4743**	0.0928	0.2570
Subexcitability	-0.0428	**0.4308**	0.1201	0.2361
TEd(40–60ms)	0.0922	-0.1285	**0.9902**	-0.1209
TEd(90–100ms)	-0.3646	-0.3611	**0.6356**	0.0956
TEd(peak)	-0.3802	0.3641	**0.5011**	-0.2838
RRP	0.3220	0.1319	-0.0691	**0.7825**
Refractoriness at 2 ms	0.3468	0.3319	0.1241	**0.6810**
Superexcitability	-0.0898	-0.2762	-0.4464	**0.6343**
Stimulus-response\slope	0.1954	0.0068	0.0397	**-0.4913**

The highest factor loading for each index were bolded. RRP: relative refractory period. SDTC: Strength-duration time constant.

R code for exploratory factor analysis

```
library(psych)
library(corrplot)
library(ggplot2)

cdataset <- scale(dataset)
cdataset <- as.data.frame(cdataset)
dat <- cdataset
X <- dat
KMO(r=cor(X))
cortest.bartlett(X)
det(cor(X))
fafitfree <- fa(dat,nfactors = ncol(X), rotate = "none")
n_factors <- length(fafitfree$e.values)
scree <- data.frame(
      Factor_n = as.factor(1:n_factors),
      Eigenvalue = fafitfree$e.values)
ggplot(scree, aes(x = Factor_n, y = Eigenvalue, group = 1)) +
      geom_point() + geom_line() +
      xlab("Number of factors") +
      ylab("Initial eigenvalue") +
      labs( title = "Scree Plot", subtitle = "(Based on the unreduced
      correlation matrix)")
fa.parallel(dat, fm="ml",fa="both", main="Parallel Analysis Scree Plots",
n.iter=1000,ylabel=NULL,show.legend=TRUE, sim=FALSE,quant=.95)
parallel <- fa.parallel(dat)

fa.none <- fa(dat, nfactors = 5, rotate="promax", fm="ml")
print(fa.none, digits=4, cutoff=.001, sort=TRUE)
fa.diagram(fa.none)
```